UNIVERSITY OF CALIFORNIA, SAN DIEGO

Luminescent tris(8-hydroxyquinolates) of Bismuth(III)

A Thesis submitted in partial satisfaction of the requirements for the degree Master of Science

in

Chemistry

by

Pauline Han

Committee in charge:

Professor William Trogler, Chair
Professor Andrew Kummel
Professor Arnold Rheingold

2012

The Thesis of Pauline Han is approved and it is acceptable in quality and form for publication on microfilm and electronically:

Chair

University of California, San Diego

2012

DEDICATION

This thesis is dedicated to my parents, thanks for giving me what I needed to succeed.

EPIGRAGH

“Don't let the fear of the time it will take to accomplish something stand in the way of your doing it. The time will pass anyway.”

TABLE OF CONTENTS

LIST OF SYMBOLS AND ABBREVIATIONS

q	8-Hydroxyquinoline
ace	acetone
ACN	acetonitrile
[A]	analyte concentration
Å	angstrom
a.u.	arbitrary units
Ar	argon
br	broad
Br	Bromine
cacld	calculated
C	carbon
CA	carboxylic acid
CCDC	Cambridge crystallographic data centre
cm	centimeter
ppm	chemical shift
Cl	chlorine
$CHCl_3$	chloroform
mm^3	cubic millimeter
^{o}	degree
deg	degrees
DFT	density functional theory

$CDCl_3$	deuterated chloroform
DCM	dichloromethane
Et_2O	diethyl ether
DMF	dimethylformamide
DMSO	dimethylsulfoxide
EDG	electron donating group
EWG	electron withdrawing group
E.A.	elemental analysis
K	equilibrium constant
EtOH	ethanol
I	fluorescence intensity
Φ	fluorescence quantum yield
fwhm	full width half maximum
g	gram
HOMO	highest occupied molecular orbital
hr	hour
H	hydrogen
I_o	initial fluorescence intensity
I	iodine
K	kelvin
L	ligand
LUMO	lowest unoccupied molecular orbital

MeOH	methanol
μL	microliter
mmol	millimole
mg	milligram
mL	milliliter
mol	mole, 6.022×10^{23}
ε	molar extinction coefficient $M^{-1}cm^{-1}$
MW	molecular weight
NO_2	nitro
OLED	organic light emitting diode
ORTEP	Oak Ridge Thermal-Ellipsoid Plot Program
c	Path length
PL	photoluminescence
π	pi, bond or orbital
π*	pi star, antibonding pi orbital
rtp	room temperature, 298K
σ	sigma, bond or orbital
σ*	sigma star, antibonding sigma orbital
√	square root
SO_3H	sulfonic acid
THF	tetrahydrafuran
TEA	triethylamine

UV	Ultra violet
UV-vis	ultra violet – visible radiation
ν	wavenumber, cm^{-1}
VSEPR	Valence shell electron pair repulsion
H_2O	water
λ_{abs}	wavelength of absorption
λ_{em}	wavelength of emission
λ_{ex}	wavelength of excitation
λ	wavelength

`

LIST OF FIGURES

LIST OF SCHEMES

LIST OF EQUATIONS

LIST OF TABLES

ACKNOWLEDGEMENTS

Thank you Professor Bill Trogler for the invaluable amount of support and guidance you've provided me.

Thank you Professor Arnie Rheingold, Curtis and Jim for all your support and assistance with this project.

Thank you Professor Dave Hendrickson and Chris Beedle for introducing me to this field as an undergraduate student.

Thank you Dr. H.P. Martinez for your assistance since the beginning.

Thank you Dr. Kristina Mitchell for being my second mentor throughout the years.

Thank you Gabe, Alex, Alissa, Phuong, Dr. Sergio Sandoval, Vincent, Dr. Kyle Grice , Kevin, Corinne for all your chemistry advice.

Thank you Drs. Nerine Cherepy and Steven Payne of Lawrence Livermore National Laboratories for the helpful discussions.

ABSTRACT OF THE THESIS

Luminescent tris(8-hydroxyquinolates) of Bismuth(III)

by

Pauline Han

Master of Science in Chemistry

University of California, San Diego, 2012

Professor William Trogler, Chair

Luminescent homoleptic bismuth(III) complexes have been synthesized by adding several functionalized 8-hydroxyquinolate ligands to bismuth(III) chloride in a 3:1 mole ratio in ethanol or tetrahydrofuran (THF). These complexes have been studied with the use of single X-ray diffraction (XRD) analysis, UV-vis spectroscopy,

fluorescence spectroscopy, and density functional theory (DFT) calculations in order to determine the structures and photophysical properties of these complexes. Solution dimerization of the mononuclear tris(hydroxyquinolate) complexes was quantified using UV-vis spectroscopy. Two dimeric compounds were characterized by single crystal X-ray analysis; bis(μ_2-5-chloro-7-iodo-8-hydroxyquinolinato)tetra(5-chloro-7-iodo-8-hydroxyquinolinato)dibismuthine and bis(μ_2-7-bromo-8-hydroxyquinolinato)tetra(7-bromo-8-hydroxyquinolinato)dibismuthine 2-tetrahydrofuran. Tris(2-(diethoxymethyl)-8-quinolinato)bismuth and triethylammonium tris(7-iodo-8-hydroxyquinolinato-5-sulfonate)bismuthate were found to be monomers in the solid state. Both compounds exhibit a higher energy emission feature, which DFT calculations assign to a transition between the HOMO (π orbital localized on the quinolate phenoxide ring) and LUMO (π orbital localized on the quinolate pyridyl ring). Both compounds showed a single emission band at low concentrations and dual emission spectra at higher concentrations. Several other compounds exhibit dual emission peaks on UV excitation that show a similar concentration dependence. UV-vis spectra of these compounds show a deviation from Beer's Law, which can be modeled as a monomer-dimer equilibrium. Excitation and emission spectra show that the monomer emits at the shorter wavelength. Electronic structure calculations support the experimental result with the HOMO-LUMO gap of 2.156 eV for the monomer significantly larger than for the dimers (1.772 eV and 1.915 eV) which correlate well with the energies of the emission peaks.

Chapter 1

Introduction

1.1 *General Introduction*

Luminescent organometallic complexes containing heavy metals have been studied for their ability to harvest both triplet and singlet excitation in organic light emitting diodes (OLEDs).[1-5] OLEDs are attractive for use in flat-panel displays because they have a low operational voltage, simple fabrication, and possess a high brightness and efficiency.[6] Metal centers such as Pt(II)and Ir(III) have shown to be highly efficient OLED emitters because their heavy atom centers facilitate singlet-triplet state mixing and intersystem crossing. Another advantage of metal complexes as emitters is the ability to readily tune their emission energies through ligand substitution. Aluminum tris-8-quinolinol (Alq_3) has been a prototypical electroluminescent metal complex, and is commercially used in OLEDS.[5] By ligand substitution, it is possible to tune the emitting wavelength through the entire visible spectrum.[7] The search for improved luminescent materials continues, as OLED displays have not yet achieved the level of reliability as LED displays. Achieving stable blue emission is often problematic for flat panel OLED applications.

Some factors that influence hydroxyquinoline ligand fluorescence include aromaticity, substitution on the aromatic ring, and structural rigidity.[5,8] An increase in rigidity leads to a decrease in electron interactions and an increase in fluorescence. The metal center also affects whether or not a complex will have either efficient fluorescence or phosphorescence. Further increasing the atomic number on a metal ion enhances the heavy atom effect or intersystem crossing (ICS), thereby increasing the likelihood of phosphorescence from the lowest excited state.[9] Additionally, the

type of metal-ligand bonding affects the emission energy of metal complexes. In hydroxyquinolate complexes, where emission originates from a ligand centered π-π* transition, a bond with a more covalent nature will shift the emission toward longer wavelengths. Conversely, an ionic metal-ligand bond will result in an emission shifted toward shorter wavelengths.[5]

In Alq_3 complexes, it is generally thought that the lowest excited states involve π-π* transitions centered on the 8-quinolate ligand that involve a net transfer of π electron density from the phenoxide ring to the pyridyl ring.[10,11] Molecular orbital calculations show that the HOMO is localized on the filled π-orbitals of the quinolate phenoxide ring whereas in the LUMO, the unfilled π* orbitals are localized on the pyridyl side of the fused ring system.[12,13] Free 8-hydroxyquinolate ligands do not normally emit strongly because of a low-lying nonradiative n-π* transition involving the phenol oxygen lone pair.[14] Metal coordination to the phenoxide oxygen raises the energy of this transition, so that the lowest excited state becomes a ligand centered π-π* transition. Several trends have been noted for Alq_3 complexes regarding ligand substitution. One example is that electron donating groups on the C-5 and C-7 positions cause a red-shift in absorption and emission wavelengths. Substitution at the C-4 or C-2 positions causes a red-shift with electron-withdrawing groups and a blue-shift with electron donating groups.[5]

An emerging use of heavy metal complex emitters is in radiation sensing using plastic scintillators. Radiation sensing is vital for the detection of illicit nuclear weapons material, toxic radionuclides potentially used in “dirty bombs,” and other

national security applications. The main focus concerning the development of new materials and improving efficiency of scintillators is to increase the radiation tolerance and maintain a high light output and transparency over several years.[15] A plastic scintillator generally contains a plastic base, a fluor, and a high-Z component. The base usually contains an aromatic group attached to a polymer backbone, such as polystyrene, while the attached dissolved fluor is an organic or inorganic emitter.[16] Organic fluorophores trap singlet excitons, whereas heavy metal emitters can trap both singlet and triplet excitatons, thereby increasing the efficiency of the plastic scintillators by as much as three-fold.[17] A high-Z component is also desirable to enhance the cross-section for interaction with γ-rays in radiation sensors. This study focuses on bismuth metal chelates that offer the potential for a high Z emitting component in plastic scintillators. Bismuth is a low cost reagent and is available in a high abundance. It also exhibits low toxicity for a heavy metal.[18,19] For radiation sensing purposes, it is also desirable that the high-Z component be highly soluble in organic polymers.[16,20] The bismuth component must also possess a wide band gap that is unable to interfere with the scintillation mechanism.[21,22] At present, relatively few luminescent complexes of bismuth(III) are known.

This study reports the synthesis of nine new homoleptic bismuth(III) complexes with functionalized 8-hydroxyquinolate ligands. The ligands are either mono- or di- substituted with differing electron withdrawing/donating properties. The structures and luminescent behaviors of the monomeric and dimeric complexes with bismuth(III) are characterized.

1.2 *Synthesis*

Various Bismuth(III) quinolates were formed by adding $BiCl_3$ to the respective 8-hydroxyquinolate ligands (Scheme 1) in ethanol and refluxed under argon.

Scheme I: L numbering scheme for BiL_3 compounds

Ligand	Compound Number (L)
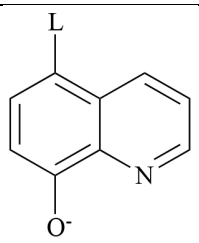	Compound **1** (L = -Cl) Compound **8** (L = $-NO_2$)
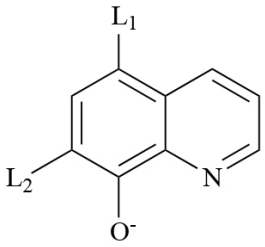	Compound **2 (**L_1, L_2 = -Cl) Compound **3** (L_1, L_2 = -I) Compound **4** (L_1 = -Cl; L_2 = -I) Compound **9** (L_1 = $-SO_3H$; L_2 = -I)
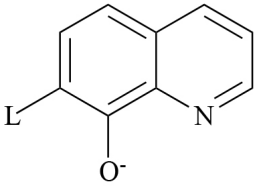	Compound **5 (**L = -Br)
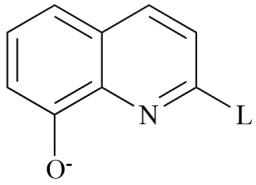	Compound **6** (L = $-C(OEt)_2$) Compound **7** (L = -COOH)

Triethylamine was added to the reaction in order to neutralize the HCl produced on metathesis of $BiCl_3$ with 8-hydroxyquinolate. *Tris(8-hydroxy-2-quinolinato-carboxylic acid)bismuth* (**7**) and *triethylammonium tris(7-iodo-8-hydroxyquinolinato-5-sulfonate)bismuthate* (**9**) were prepared in THF solvent, because their respective 8-hydroxyquinolate ligand precursors were insoluble in ethanol. After vacuum filtration and subsequently drying under vacuum for 24-48 h, compounds with an approximate BiL_3 stoichiometry were obtained. With the exception of *tris(5,7-diiodo-8-hydroxyquinolinato)bismuth* (**3**) and *tris(8-hydroxy-5-nitroquinolinato)bismuth* (**8**), all the other compounds were moderately soluble in common polar and aromatic solvents (including chloroform, CH_2Cl_2, ethyl acetate, THF and toluene) and insoluble in hydrocarbons (pentanes and hexanes). Compounds **3** and **8** were insoluble in the above solvents. All compounds, however, were soluble in the polar donor solvent DMF. *Tris(5-chloro-8-hydroxyquinolinato)bismuth* (**1**), *tris(5,7-dichloro-8-hydroxyquinolinato)bismuth* (**2**), and *tris(8-hydroxy-5-nitroquinolinato)bismuth* (**8**) formed yellow powders on recrystallization from warm THF and layering with hexanes. *Bis(μ_2-5-chloro-7-iodo-8-hydroxyquinolinato)tetra(5-chloro-7-iodo-8-hydroxyquinolinato)dibismuthine* (**4**), and *tris(2-(diethoxymethyl)-8-quinolinato)bismuth* (**6**) were recrystallized successfully from THF/hexanes and formed dark brown and light yellow crystals, respectively. *Bis(μ_2-7-bromo-8-hydroxyquinolinato)tetra(7-bromo-8-hydroxyquinolinato)dibismuthine 2-tetrahydrofuran* (**5**), was recrystallized from CH_2Cl_2/hexanes and formed large brown crystals. Compound **9** was initially

crystallized in its protonated form from THF; however, the soft crystals obtained were amorphous and could not be used for X-ray diffraction analysis. The compound was therefore recrystallized as the ammonium salt by the addition of triethylamine in THF solvent to deprotonate the sulfonic acid groups.

Emission spectra were observed for compounds **2, 4, 5,** and **6** in degassed CH_2Cl_2 at high and low concentrations at 298K. The solid-state compounds were first dried under vacuum and then were dissolved in solution. The emission spectra were taken for these compounds in CH_2Cl_2 at the recorded concentrations. The solutions were then degassed with argon for 20 min and the color of the solutions did not change. The emission spectra of degassed solutions did not show a change in intensity of the emission peaks, indicating that dioxygen does not efficiently quench the emission in solution.

Chapter 2.

Molecular Structures of BiL_3 Compounds.

2.1 *Molecular structure of bis(μ_2-5-chloro-7-iodo-8-hydroxyquinolinato)tetra(5-chloro-7-iodo-8-hydroxyquinolinato)dibismuthine (**4**).*

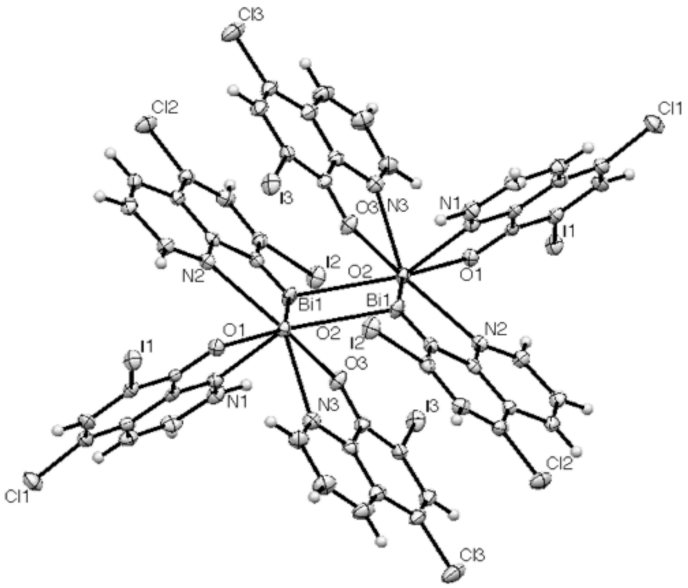

Figure 1. a.) ORTEP representation of compound **4**. Probability ellipsoids are drawn at 50% level. For clarity, lattice solvent is omitted.

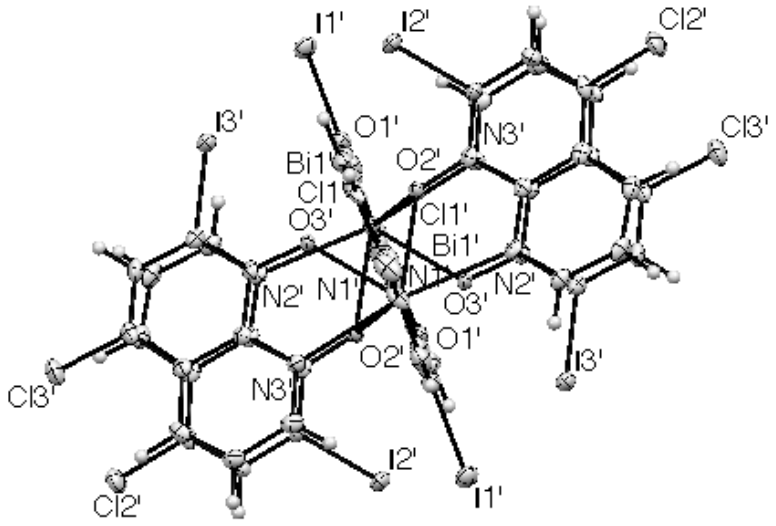

Figure 1. b.) Plot showing eclipsed π stacking of the quinolate rings when viewed from above the rings.

Compound **4** (Figure **1**) is dimeric and each metal center is 7-coordinate with an approximate pentagonal bipyrimidal geometry. It has been noted that if stereochemically active lone pairs are taken into account, the structure of many bismuth(III) compounds can be regarded as 8-coordinate with a distorted dodecahedral geometry.[23-25] Selected bond lengths and angles are reported in Tables **1** and **2**. The Bi1-N1 bond has a significantly shorter bond length of 2.352Å when compared to the other Bi-N bonds. This is most likely due to the fact that the axial quinolate is perpendicular to the other two quinolate ligands and is in an environment with little steric crowding. All three Bi-O bonds are very similar in length.

Due to the Lewis acidity of the metal center, the crystal structure (Figure **1**) shows that each bismuth is bridged to one of the 5-chloro-7-iodo-8-hydroxyquinolate ligands via an oxygen donor atom from a ligand on the adjacent bismuth. This structure shows that the four equatorial quinolate ligands in the dimer exhibit π-stacking with the phenoxide rings eclipsing the pyridyl rings. Since the HOMO is a π-type orbital localized on the phenoxide portion of the hydroxyquinolate and the LUMO is a π-type orbital more localized on the pyridyl ring of the hydroxyquinolate ligand this may give rise to a donor-acceptor type of π-interaction that contributes to the stability of the dimeric structure.

Table 1. Selected bond distances (Å) in compound **4**.

Bi(1)-O(1)	2.295(3)	**Bi(1')-O(3')**	2.299(3)
Bi(1)-O(3)	2.320(3)	**Bi(1')-O(1')**	2.306(3)
Bi(1)-O(2)	2.329(3)	**Bi(1')-O(2')**	2.322(3)
Bi(1)-N(1)	2.352(4)	**Bi(1')-N(1')**	2.332(4)
Bi(1)-N(3)	2.582(4)	**Bi(1')-N(3')**	2.587(4)
Bi(1)-N(2)	2.590(4)	**Bi(1')-N(2')**	2.658(4)
Bi(1)-Bi(1)#1	3.5683(4)	**Bi(1')-Bi(1')#2**	3.6035(4)

Table 2. Selected bond angles (deg) in compound **4**.

O(1)-Bi(1)-O(3)	134.79(12)	**O(3)-Bi(1)-N(2)**	128.74(12)
O(1)-Bi(1)-O(2)	137.31(11)	**O(2)-Bi(1)-N(2)**	66.21(11)
O(3)-Bi(1)-O(2)	65.62(12)	**N(1)-Bi(1)-N(2)**	74.96(13)
O(1)-Bi(1)-N(1)	70.94(13)	**N(3)-Bi(1)-N(2)**	148.73(12)
O(3)-Bi(1)-N(1)	80.27(13)	**O(1)-Bi(1)-Bi(1)**	163.38(8)
O(2)-Bi(1)-N(1)	79.66(13)	**O(3)-Bi(1)-Bi(1)**	57.91(9)
O(1)-Bi(1)-N(3)	75.86(12)	**O(2)-Bi(1)-Bi(1)**	53.07(8)
O(3)-Bi(1)-N(3)	66.18(12)	**N(1)-Bi(1)-Bi(1)**	125.46(10)
O(2)-Bi(1)-N(3)	130.60(12)	**N(3)-Bi(1)-Bi(1)**	106.95(9)
N(1)-Bi(1)-N(3)	82.37(13)	**N(2)-Bi(1)-Bi(1)**	103.72(9)
O(1)-Bi(1)-N(2)	76.54(12)		

2.2 *Molecular Structure of bis(μ_2-7-bromo-8-hydroxyquinolinato)tetra(7-bromo-8-hydroxyquinolinato)dibismuthine 2-tetrahydrofuran (**5**).*

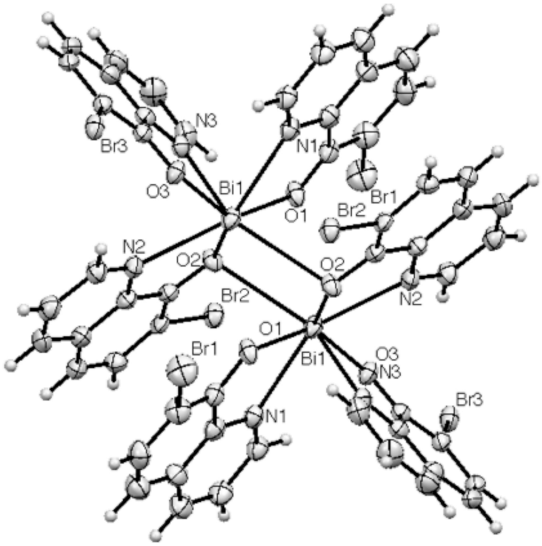

Figure 2. ORTEP representation of compound **5**. Probability ellipsoids are drawn at 50% level. For clarity, lattice solvent is omitted.

The dark brown crystal (0.33 x 0.29 x 0.23mm^3) was measured at room temperature. X-ray diffraction analysis (Figure **2**) shows that compound **5** has three coordinated 7-bromo-8-quinolinol chelates on each metal center. The compound is crystallized with one molecule of THF solvent that is disordered. The compound is a dimer, which is isostructural with compound **4**. Selected bond lengths and angles are reported in Tables **3** and **4**. The axial Bi1-N3 (2.335Å) bond distance is significantly shorter compared to the other equatorial Bi-N (2.585, 2.603Å) bonds. Although compound **5** is mostly isostructural to compound **4,** it has slightly (±0.05) different bond lengths due to different steric hindrances from the substituted quinolinols. The Bi-O distances on all three ligands are all similar to each other and in the range of (2.303-2.331Å). The bridging Bi-O1 bond lengths are significantly longer at 2.8703Å, due to the fact that they have the bridging interaction between two separate monomers. The π-stacking of the quinolinol ligands is the same as in the structure of **4**.

.

Table 3. Select bond distances (Å) in compound **5**.

Bi1-O2	2.303	**Bi1-N2**	2.585
Bi1-O3	2.328	**Bi1-N1**	2.603
Bi1-O1	2.331	**Bi-Bi**	2.674
Bi1-N3	2.335		

Table 4. Select bond angles (deg) in compound **5**

O2-Bi1-O3	134.1	**O3-Bi1-N1**	77.1
O2-Bi1-O1	66.6	**O1-Bi1-N1**	65.9
O3-Bi1-O1	1374	**N3-Bi1-N1**	76.6
O2-Bi1-N3	79.8	**N2-Bi1-N1**	148.5
O3-Bi1-N3	70.9	**O2-Bi1-Bi1**	51.6
O1-Bi1-N3	80.4	**O3-Bi1-Bi1**	162.38
O2-Bi1-N2	67.1	**O1-Bi1-Bi1**	58.97
O3-Bi1-N2	74.3	**N3-Bi1-Bi1**	124.8
O1-Bi1-N2	132.5	**N2-Bi1-Bi1**	98.5
N3-Bi1-N2	81.9	**N1-Bi1-Bi1**	112.6
O2-Bi1-N1	129.5		

2.3 *Molecular Structure of tris(2-(diethoxymethyl)-8-quinolinato)bismuth* (**6**).

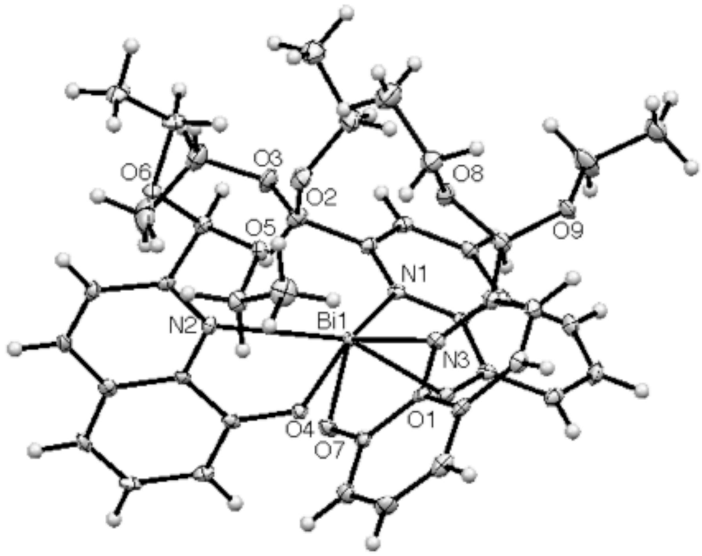

Figure 3. ORTEP representation of compound **6.** Probability ellipsoids are drawn at the 50% level.

The yellow-orange crystal (0.25 mm x 0.22 mm x 0.20mm) was measured at room temperature. The compound (Figure **3**) has a 6-coordinate metal center chelated by three quinolinol ligands. The structure is a squashed octahedral geometry with a *fac*-arrangement of the hydroxypyridinate ligand. The octahedral geometry is distorted due to the narrow bite of the 5-membered chelate ring, as well as the stereochemically bulky acetal substituents. The metal center can be regarded as a 7-coordinate species with pseudo C_3 symmetry with a stereochemically active lone pair extending along the C_3 axis toward the empty pocket formed by the acetal ligands. It should be noted that Alq_3 species generally favor the meridional (C_1) structure,[10,11,26,27] in contrast to the facial (C_3) geometry about bismuth(III).

Select bond angles and distances are given in Tables **5** and **6**. The expansion of the three nitrogen bond angles can also be explained by the placement of a stereochemically active lone pair, which faces towards the acetal "pocket". The *cis*-N1-N3-N2 angles are expanded to make room for the lone pair. The N1-Bi-N2 bond angle is increased to 106.84°, the N3-Bi-N1 angle to 117.15°, and the N3-Bi-N2 angle to 130.98°. The Bi-N bonds have a range between 2.591-2.666 Å. The Bi-N3 bond distance(2.591Å), which would otherwise be the terminal ligand in the dimers, has the shortest bond length among the three Bi-N bonds. The three *cis*-oxygen bond angles are concomitantly decreased due to the lengthening of the bonds from the metal center to nitrogen. The angles are summarized in Table **6**. The Bi-O bond lengths range between 2.183-2.127 Å, which is consistent with strong coordination. Crystal packing

shows no close contact from other ligands; the closest atoms are 3.972 Å apart from each other.

Table 5. Select bond distances (Å) in compound **6**.

Bi1-O7	2.183	**Bi1-N3**	2.591
Bi1-O4	2.196	**Bi1-N1**	2.624
Bi1-O1	2.217	**Bi1-N2**	2.666

Table 6. Select bond angles (deg) of compound **6**.

O7-Bi1-O4	81.52	**O1-Bi1-N1**	67.81
O7-Bi1-O1	87.69	**N3-Bi1-N1**	117.15
O4-Bi1-O1	81.72	**O7-Bi1-N2**	84.6
O7-Bi1-N3	68.77	**O4-Bi1-N2**	67.84
O4-Bi1-N3	140.6	**O1-Bi1-N2**	149.36
O1-Bi1-N3	72.09	**N3-Bi1-N2**	130.98
O7-Bi1-N1	149.29	**N1-Bi1-N2**	106.84
O4-Bi1-N1	77.01		

2.4 *Molecular Structure of triethylammonium tris(7-iodo-8-hydroxyquinolinato-5-sulfonate)bismuthate* (**9**).

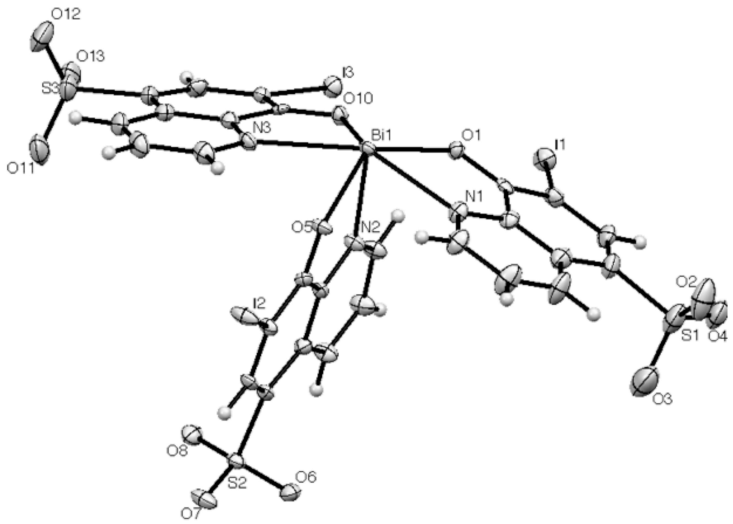

Figure 4. a.) ORTEP representation of compound **9**. Probability ellipsoids are drawn at the 50% level. Lattice solvent and triethylammonium ions have been omitted for clarity.

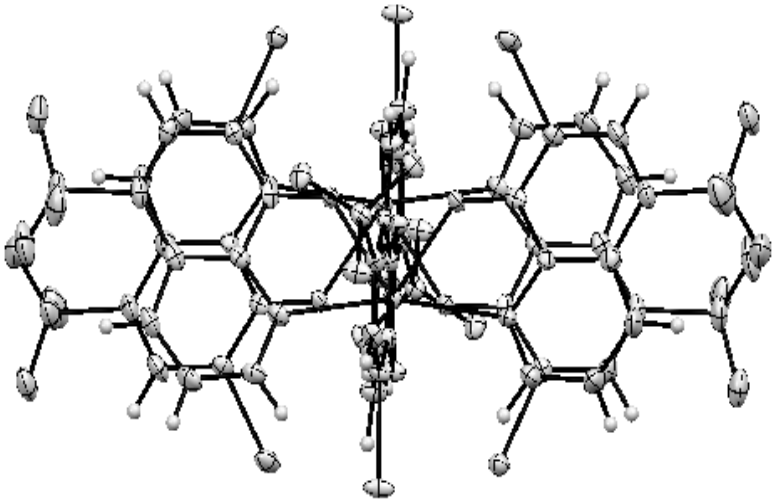

Figure 4. b.) Plot of adjacent molecules in the crystal that indicate a π-stacking interaction similar to that found in the related dimers

The light yellow crystal (0.22 x 0.14 x 0.10mm^3) was measured by X-ray diffraction at room temperature. The compound (Figure **4**) has four disordered triethylammonium cations that counterbalance the anionic sulfonate groups. There are also two disordered ethanol molecules of crystallization. Single crystal X-ray diffraction analysis reveals that the metal center is 6-coordinate with three chelating 7-iodo-8-quinolinol-5-sulfonic acid ligands. Although the bismuth center is 6-coordinate with a distorted octahedral geometry, the arrangement of the quinolate ligands is very similar to that in the dimeric compounds **4** and **5**. Select bond angles and distances are given in Tables **7** and **8**. The Bi-N2 bond in the axial chelate (2.346Å) trans to the lone pair is significantly shorter than the other two Bi-N1 and Bi-N3 bonds (2.514, 2.536Å). However, all the Bi-N bond distances are distinctly longer than the sum of the atomic radii, implying a weakly coordinated Bi-N bond. The Bi-O distances are close to the sum of their atomic radii, indicative of a strong bond.

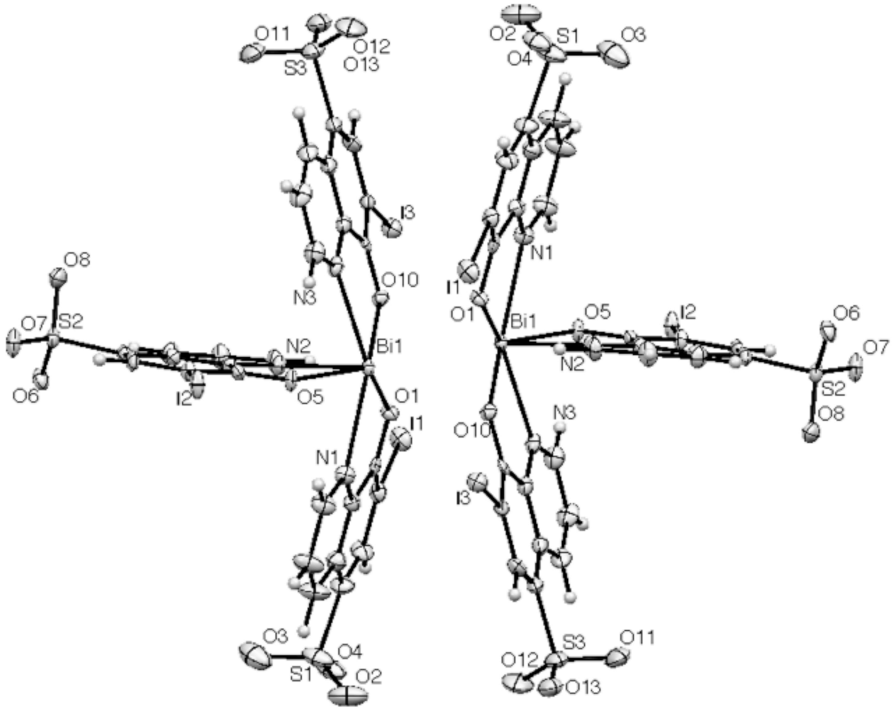

Figure 5. Crystal packing diagram of compound **9**. Probability ellipsoids are drawn at 50% level. Lattice ethanol and triethylammonium ions have been omitted for clarity.

The crystal packing diagram of compound **9** (Figure **5**) shows an interesting stacking arrangement similar to that found in compounds **4** and **5**. The equatorial hydroxyquinolate in adjacent molecules are approximately parallel to each other even though there is no bridging ligand. The bismuth centers are staggered somewhat to avoid repulsion. The Bi-Bi bond separation is 3.670Å, which is much longer than a typical dibismuthine bond (3.00Å). The inter-ligand Bi-O bond distances are 2.960 Å, which is significantly longer than the Bi-O bonds seen in the previous dimers. This dinuclear arrangement, however, exhibits π-stacking similar to that seen in the other dimers that contain oxygen bridging. The arrangement of the complexes in Figure **5** further suggests that there is π-stacking between the quinolinol rings may be a stabilizing factor in this class of compounds. In this compound the stacked quinolate ligands are splayed back slightly to accommodate the bulky repulsive anionic sulfonate substitutents on the 5 position of the quinolate ring.

Table 7. Select bond distances (Å) of compound **9**.

Bi1-O10	2.316	**I1-C3**	2.103
Bi1-O1	2.32	**I2-C12**	2.091
Bi1-O5	2.321	**I3-C21**	2.097
Bi1-N2	2.346	**S1-C5**	1.771
Bi1-N1	2.514	**S2-C14**	1.779
Bi1-N3	2.536	**S3-C23**	1.787
Bi-Bi	3.6701		

Table 8. Select bond angles (deg) of compound **9**.

O10-Bi-O1	69.66	**O5-Bi-N1**	73.59
O10-Bi-O5	129.46	**N2-Bi-N1**	81.07
O1-Bi-O5	131.78	**O10-Bi-N3**	67.71
O10-Bi-N2	74.72	**O1-Bi-N3**	136.03
O1-Bi-N2	74.6	**O5-Bi-N3**	72.66
O5-Bi-N2	70.16	**N2-Bi-N3**	82.55
O10-Bi-N1	134.63	**N1-Bi-N3**	145.8
O1-Bi-N1	67.63		

2.5 *Summary of Molecular Data*

Table 9. Crystollagraphic data and refinement information for compounds **4, 5, 6, 9**

Compound Formula	**4** $C_{57}H_{20}Bi_2Cl_{12}I_6N_6O_6$	**5** $C_{31}H_{23}BiBr_3N_3O_4$	**6** $C_{42}H_{48}BiN_3O_9$	**9** $C_{47}H_{66}BiI_3N_6O_{13}S_3$
fw	2499.63	950.23	947.81	1608.92
Space group (crystal system)	P-1 (Triclinic)	R-3 (Rhombohedral)	$P2_1/c$ (Monoclinic)	P-1 (Triclinic)
Lattice Parameters: a/ b/ Å	12.6366 (7) 14.5777(7)	40.5434(17) 40.5434(17)	16.6906 (6) 15.6114 (6)	12.36 15.926
c/Å	18.8823 (10)	11.0916 (4)	14.9353 (6)	16.503
α/deg	87.431 (2)	90	90	111.787
β/deg	88.934 (2)	90	97.5270 (10)	107.069
γ/deg	74.979 (2)	120	90	95.822
V/Å^3	3356.0 (3)	15789.4 (11)	3858.1 (3)	2801.6
Z Value	2	18	4	2
D_c/gcm^{-3}	2.474	1.799	1.623	1.907
μ/mm^{-1} (MoK_{alpha})	8.528	8.477	4.631	4.976
Temp (K)	100	100	100	100
$2\Theta_{max}$/deg	55.08	50.76	56.62	53.08
No. Rflns Measd	71652	45033	35840	40955
No. Rflns Used (R_{int})	15379 (0.0340)	6405 (0.0675)	9475 (0.0558)	11517 (0.0343)
No. Parameters	819	354	496	673
Final R (I>2σ(I)): R1:wR2	0.0285: 0.0604	0.0330: 0.0812	0.0288:0.0619	0.0306: 0.0607
R(all data): R1:wR2	0.0413: 0.0652	0.0407: 0.0843	0.0407: 0.0667	0.0424: 0.0647
Goodness of fit on F^2	1.031	1.032	1.036	1.028
Largest Peak	1.517	1.563	2.203	1.13
Deepest Hole	-2.268	-0.669	-0.958	-0.97

Chapter 3

UV-Vis Spectroscopy

3.1 *Absorption Spectra at Varying Concentrations*

The absorption spectra for compounds **2, 4, 5,** and **6** were observed at various concentrations in 1mm and 1cm path length cuvettes**.** The compounds were first dried under vacuum for 24-48 h and then dissolved in CH_2Cl_2 at 298K. Figure **6** shows the absorption spectra for compound **2.** The absorption at 401 nm exhibits a deviation from linearity (Beer's Law) when various concentrations are plotted against their absorbance values (Table **10**). The absorption spectra for compound **4** (Figure **7**) show four absorption bands at low concentration at 247, 305, 368, and 408 nm. The lowest energy absorption at 408 nm (Table **11**) was used to determine whether or not compound **4** obeys Beer's law. The intensity of the long wavelength absorption in **2** and **4** did not increase linearly with the concentration. The absorbance at 385 nm (Table **12**) for compound **5** (Figure **8**) behaves similarly. Compound **4** exhibits new peaks 265 nm and 391 nm as the concentration increases. Both show a deviation from Beer's law. Given the tendency of the hydroxyquinolate complexes of bismuth(III) to dimerize in the solid state, this could be an indication of a solution equilibrium that shifts from the monomeric to the dimeric form at increasing concentrations.[28] This would explain the appearance of new spectral features at higher concentrations.

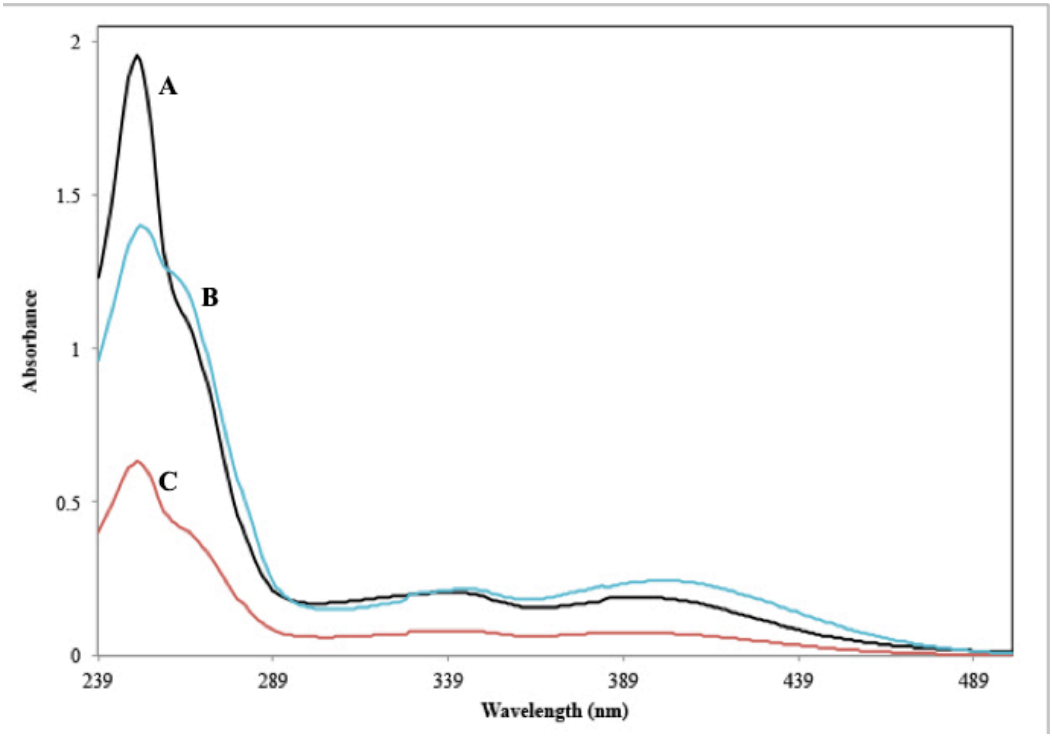

Figure 6. Electronic absorbance spectra of tris(5,7-dichloro-8-hydroxyquinolinato)bismuth (Compound **2**) in CH_2Cl_2 at 298K. A, [**2**] = 3.19 x 10^{-5}M, path length = 6.26 mm. B, [**2**] = 2.07 x 10^{-4}M, path length = 1 mm. C, [**2**] = 6.90 x 10^{-5}M, path length = 6.26 mm.

Table 10. Absorbance values of tris(5,7-dichloro-8-hydroxyquinolinato)bismuth (Compound 2) at 401 nm.

	Concentration (M)	Absorbance	ε ($M^{-1}cm^{-1}$)
A	3.19 x 10^{-5}M	0.0306	153
B	2.07 x 10^{-4}	0.2443	1180
C	6.90 x 10^{-5}	0.0723	167

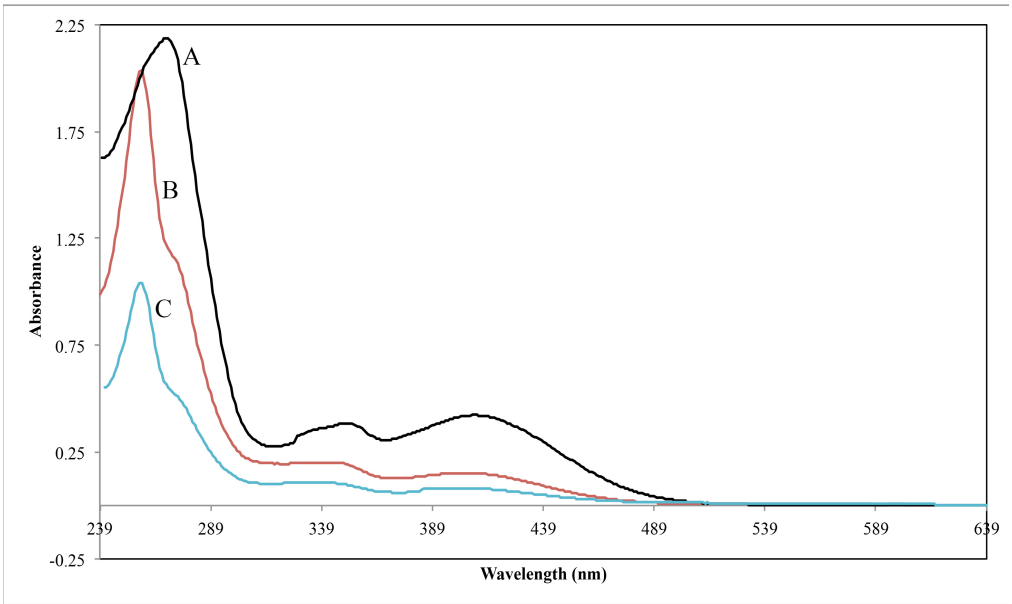

Figure 7. Electronic absorbance spectra of bis(μ_2-5-chloro-7-iodo-8-hydroxyquinolinato)tetra(5-chloro-7-iodo-8-hydroxyquinolinato)dibismuthine (Compound **4**) in CH_2Cl_2 at 298K. A, [**4**] = 1.34 x 10^{-5} M, path length = 1 mm. B, [**4**] = 5.48 x 10^{-6} M, path length = 6.25 mm.[29] C, [**4**] = 3.89 x 10^{-7}M, path length = 6.25 mm.

Table 11. Absorbance values of bis(μ_2-5-chloro-7-iodo-8-hydroxyquinolinato)tetra(5-chloro-7-iodo-8-hydroxyquinolinato)dibismuthine (Compound **4)** at 408 nm.

	Concentration (M)	Absorbance	**ε** ($M^{-1}cm^{-1}$)
A	1.24 x 10^{-5}	0.4228	4987
B	5.48 x 10^{-6}	0.1508	1634
C	3.87 x 10^{-7}	0.0837	34338

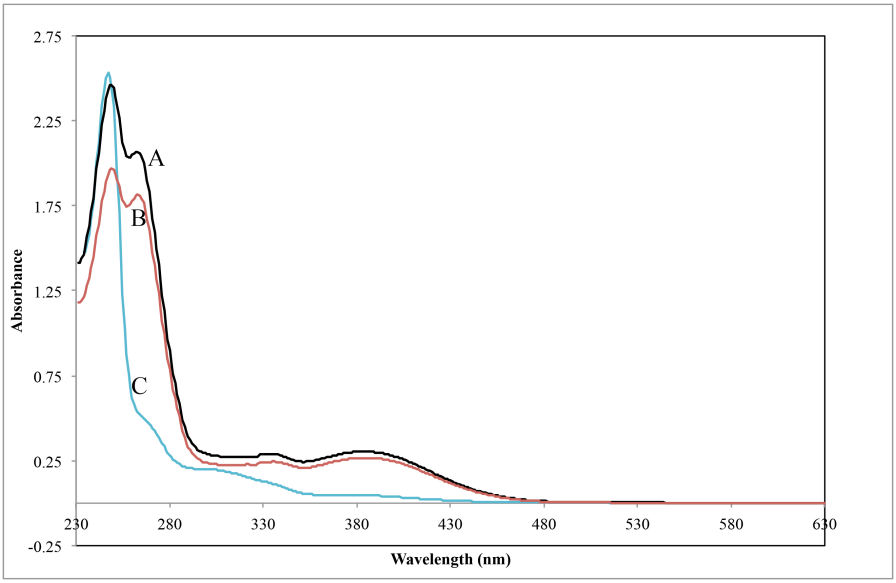

Figure 8. Electronic absorption spectra of bis(μ_2-7-bromo-8-hydroxyquinolinato)tetra(7-bromo-8-hydroxyquinolinato)dibismuthine 2-tetrahydrofuran (Compound **5**) in DCM at 298K. A, [**5**] = 2.16 x 10^{-4}M, path length = 1 mm. B, [**5**] = 1.26 x 10^{-4}M, path length = 1 mm. C, [**5**] = 1.54 x 10^{-5}M, path length = 6.22 mm.[29]

Table 12. Absorbance values of 1 bis(μ_2-7-bromo-8-hydroxyquinolinato)tetra(7-bromo-8-hydroxyquinolinato)dibismuthine 2-tetrahydrofuran (Compound **5**) at 385 nm.

	Concentration (M)	Absorbance	ε ($M^{-1}cm^{-1}$)
A	2.16 x 10^{-4}	0.2675	1401
B	1.26 x 10^{-4}	0.2671	2121
C	1.54 x 10^{-5}	0.0463	508

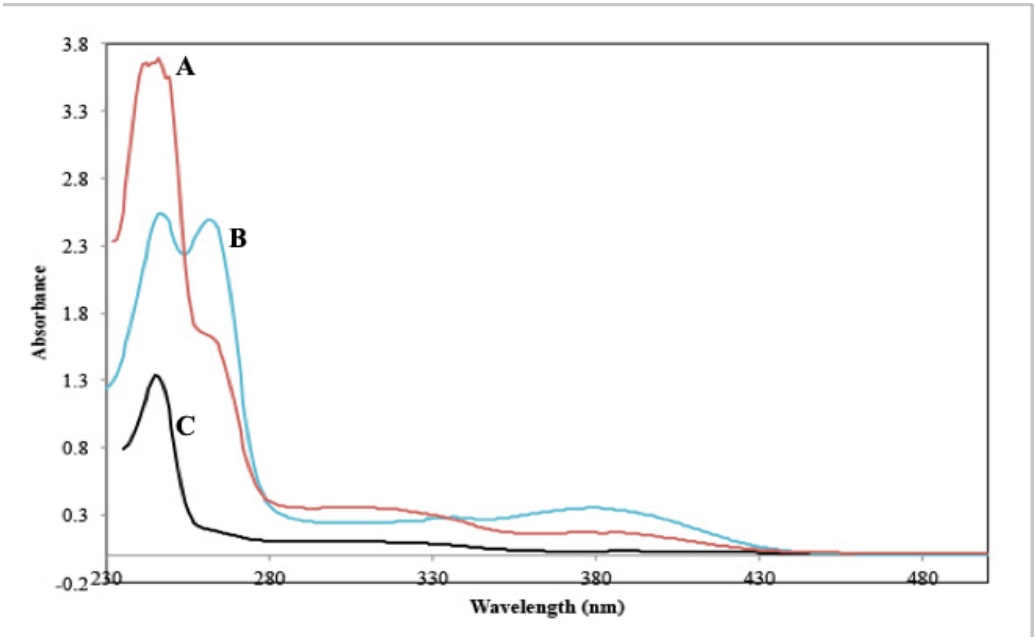

Figure 9. Electronic absorption spectra of tris(2-(diethoxymethyl)-8-quinolinato)bismuth (compound **6**) in CH_2Cl_2 at 298K. A, [**6**] = 5.08 x 10^{-5}M, path length = 6.07mm. B, [**6**] = 3.60 x 10^{-4}M, path length = 1 mm. C, [**6**] = 1.39 x 10^{-5}M, path length = 6.07 mm

Table 13. Absorbance values of tris(2-(diethoxymethyl)-8-quinolinato)bismuth (compound **6**) at 391 nm

	Concentration (M)	Absorbance	ε ($M^{-1}cm^{-1}$)
A	5.08 x 10^{-5}	0.1643	533
B	3.60 x 10^{-4}	0.3257	905
C	1.39 x 10^{-5}	0.03418	404

3.2 *Monomer Dimer Exchange Equilibrium*

The deviations from Beer's law can be modeled as the monomer-dimer equilibrium shown in equation 1.

$$2\ BiX_3 \overset{K}{\rightleftharpoons} [BiX_3]_2 \qquad \text{(Eq. } \mathbf{1}\text{)}$$

In equation **1**, $[BiX_3]_2$ is the dimeric form of BiX_3 and X is one of the ligands **1-9**. The √absorbance was plotted against $[BiX_3]$/√absorbance in order to model this equilibrium.[30] Figures **10, 11, 12,** and **13** establish the equilibrium dependence for compounds **2, 4**, **5,** and **6**, respectively. The linearity of each of the plots is consistent with a dynamic monomer-dimer equilibrium. The conversion from monomer to dimer is modeled[30] by the following parameters: slope = $(2/\varepsilon_2)$ and y –intercept = $1/\sqrt{(\varepsilon_2 * K)}$. The values found for ε_2 and K at different absorbance values for compounds **2, 4, 5** and **6** are given in Table **14**.

Table 14. $\varepsilon_{2,}$ and K values for compounds **2, 4**, **5,** and **6**. The absorbances were monitored for compound **2** at 401 nm, for compound **4** at 408 nm, for compound **5** at 385 nm, and for compound **6** at 391 nm

	2	**4**	**5**	**6**
ε_2	$2.9 \pm 0.8 \times 10^{3}$	$6.4 \pm 0.7 \times 10^{3}$	$2.6 \pm 0.1 \times 10^{4}$	$2.7 \pm 0.2 \times 10^{3}$
K	$8.2 \pm 1.2 \times 10^{4}$	$8.3 \pm 2.9 \times 10^{4}$	$1.5 \pm 0.3 \times 10^{5}$	$1.2 \pm 0.2 \times 10^{4}$

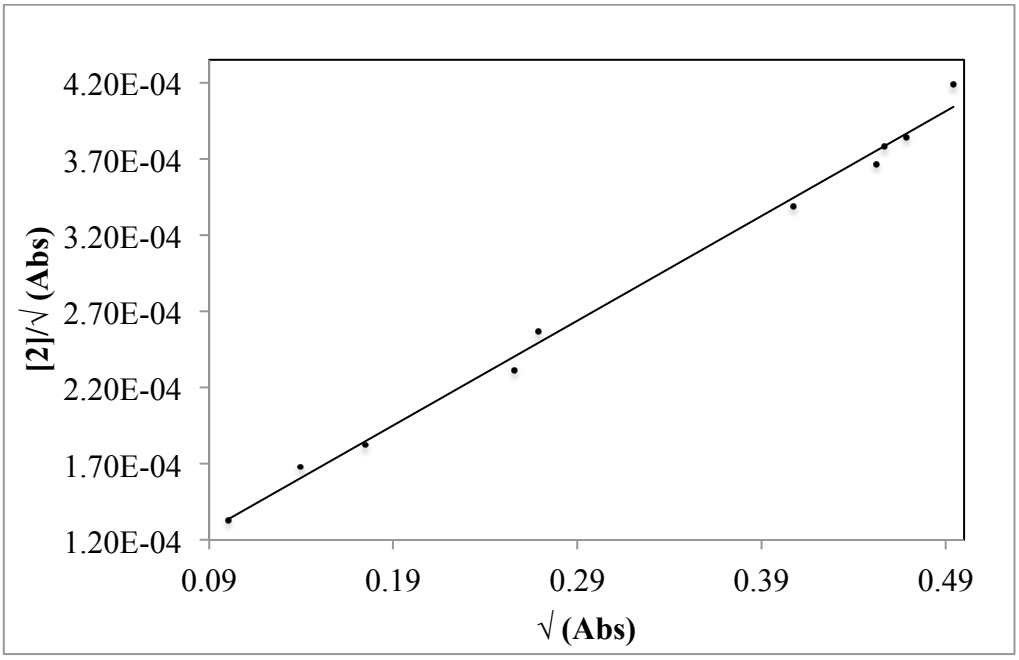

Figure 10. Plot of [**2**]/$A_{401}^{1/2}$ vs $A_{401}^{1/2}$ over the concentrations from 2.07 x 10^{-4} M to 1.34 x 10^{-5} M. The absorbance was measured in CH_2Cl_2 at 298K and 401 nm.

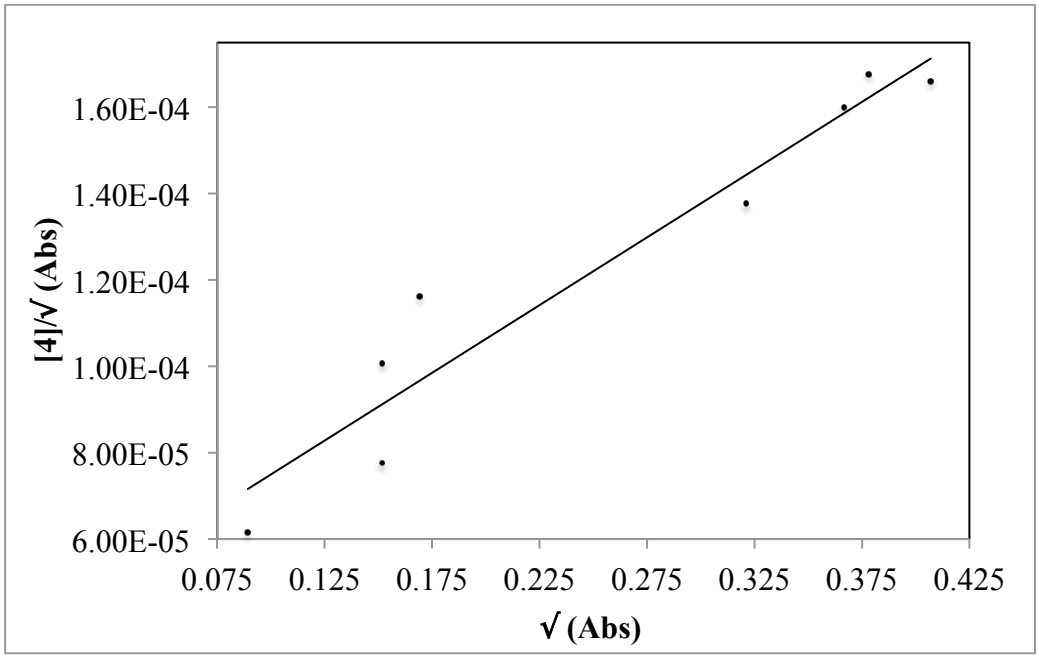

Figure 11. Plot of [**4**]/$A_{408}^{1/2}$ vs $A_{408}^{1/2}$ over the concentration range from 1.18 x 10^{-5} M to 6.75 x 10^{-5} M. The absorbance was measured in CH_2Cl_2 at 298K and 408 nm.

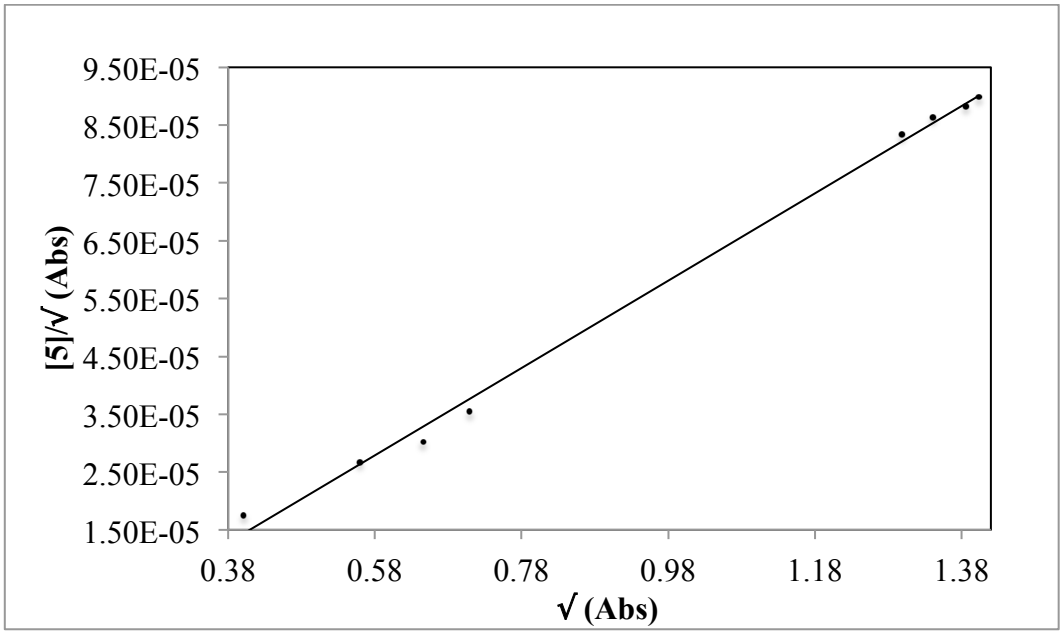

Figure 12. Plot of [**5**]/$A_{385}^{1/2}$ vs $A_{385}^{1/2}$ over the concentration range from 1.082 x 10^{-4} M to 7.008 x 10^{-6} M. The absorbance was measured in CH_2Cl_2 at 298K and 385 nm.

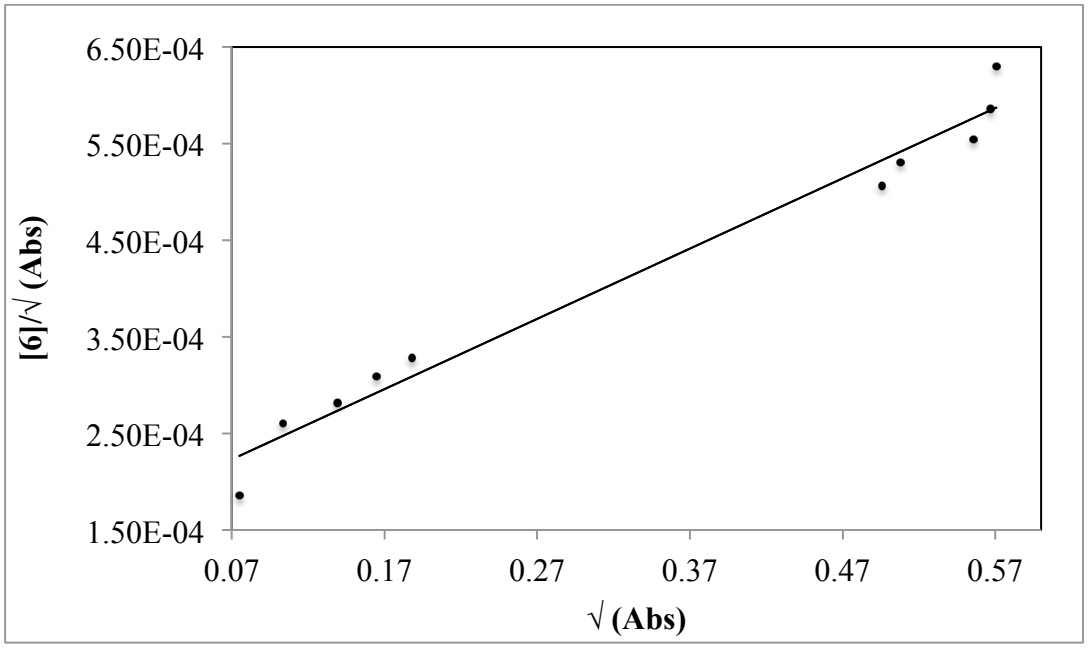

Figure 13. Plot of [**6**]/$A_{391}^{1/2}$ vs $A_{391}^{1/2}$ over the concentration range from 2.07 x 10^{-4} M to 1.34 x 10^{-5}M. The absorbance was measured in CH_2Cl_2 at 298K and 391 nm.

The deviation from Beer's Law observed and high equilibrium constants obtained for compounds **4** and **5** is consistent with a solution equilibrium between the monomer and dimer forms. Compounds **2** and **6** exhibit a lower dimerization equilibrium constant, but still exhibit deviations from Beer's Law behavior at modest concentrations. It is likely that such solution equilibria exist to some extent for most hydroxyquinolinate complexes of bismuth(III). It is noteworthy that the compounds crystallized as dimeric complexes were the ones with the highest equilibrium constants for dimerization according to the solution absorption spectral measurements.

Chapter 4

Fluorescence Spectroscopy

4.1 *Emission Spectra of Tris(hydroxyquinolato) Complexes of Bismuth(III)*

Tris-(8-hydroxyquinolato)aluminum (Alq_3) displays a characteristic green emission and is frequently used as the electron transport and emitting layer in efficient low molecular weight OLEDS.[11] Molecular orbital studies show that the HOMO orbitals are π-type and localized on the phenoxide ring of the quinolate ligand, while the LUMO is a π*-orbital more localized on the pyridyl ring. It was also shown that the lowest singlet state seen in absorption is a π-π* transition primarily centered on the quinolate ligands.[10,11,26,31] In Alq_3, the compound exhibits a green emission band at 556 nm.[32] The fluorescence spectra for tris(8-hydroxyquinoline)bismuth (Biq_3) was examined previously and found to exhibit room temperature emission at 540 nm.[22] This emission peak was also assigned a ligand-localized fluorescence that is not associated with the heavy atom bismuth.

The emission spectra of all compounds in the present study were observed at room temperature (298K). The compounds were first dried under vacuum for 24-48 h and added to their respective solvents (Table **15**). Table **15** also includes all the photoluminescent properties of each compound. Compound **2** (Figure **14**) contains a single emission broad peak at 525 nm with a full width at half maximum (fwhm) of 73 nm. According to Chen and Shi, the addition of halogen groups to the 5- position of the quinolinol ring will blue-shift the emission of the compound.[5] The addition of two chlorine groups on the 5- and 7- position of the 8-quinolate rings (**2**) follows this rule and slightly blue shifts the emission peak by 25 nm. The lowest singlet absorption of this compound can be similarily assigned a π-π* transition on the ligand (involving

charge transfer from the phenoxide ring to pyridyl ring). The blue-shifted emission observed for these compounds can be attributed to the π-electron donating power of the halogens in the 5- and 7- positions on the quinolate ligand.

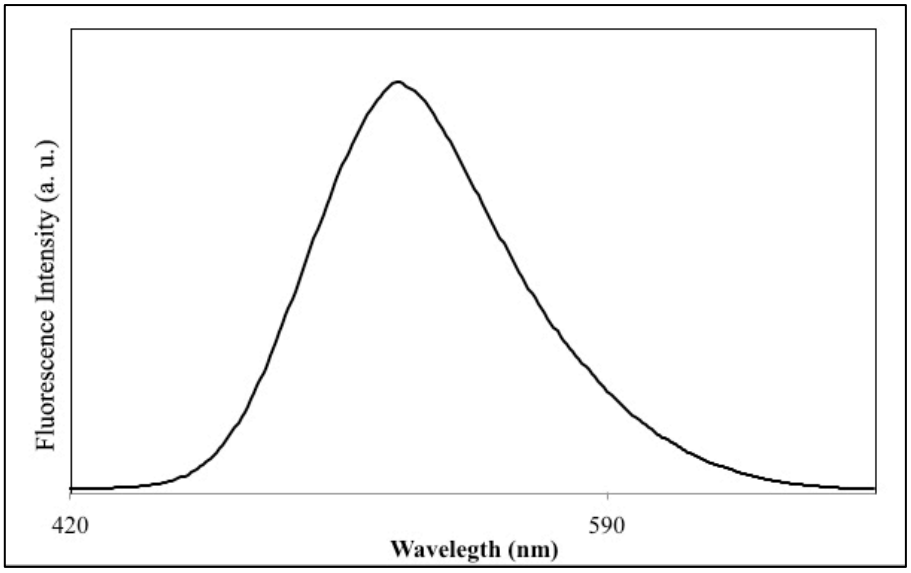

Figure 14. Fluorescence spectrum of tris(5,7-dichloro-8-hydroxyquinolinato)bismuth (**2**). The spectrum was taken in DMF at 298K and the excitation wavelength was 350 nm.

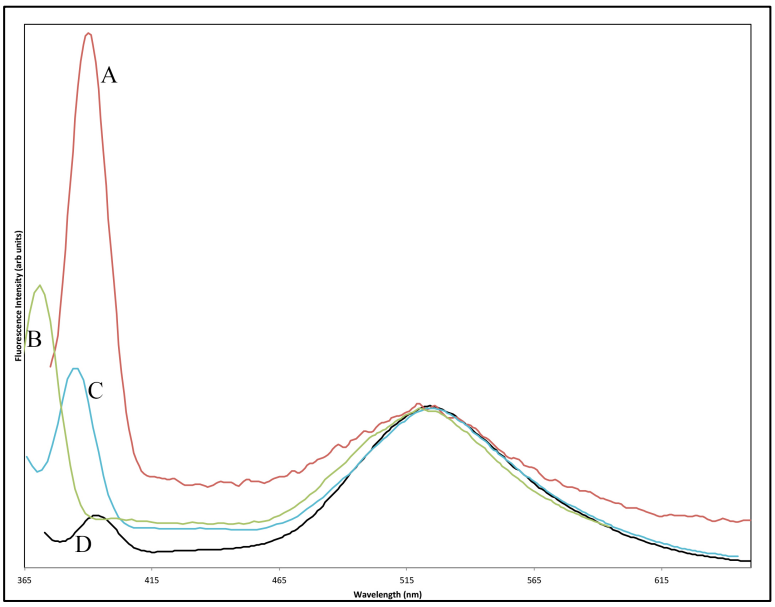

Figure 15. Emission spectra of A, bis(μ_2-7-bromo-8-hydroxyquinolinato)tetra(7-bromo-8-hydroxyquinolinato)dibismuthine 2-tetrahydrofuran (Compound **5**) at excitation wavelength 354 nm; B, tris(5,7-diiodo-8-hydroxyquinolinato)bismuth (Compound **3**) at excitation wavelength 354 nm; C, tris(8-hydroxy-2-quinolinato-carboxylic acid)bismuth (Compound **7**) at excitation wavelength 346 nm; D, bis(μ_2-5-chloro-7-iodo-8-hydroxyquinolinato)tetra(5-chloro-7-iodo-8-hydroxyquinolinato)dibismuthine (Compound **4**) att excitation wavelength 352 nm. Spectrum A was taken in CH_2Cl_2 at 298K, spectra B, C and D were taken in DMF at 298 K.

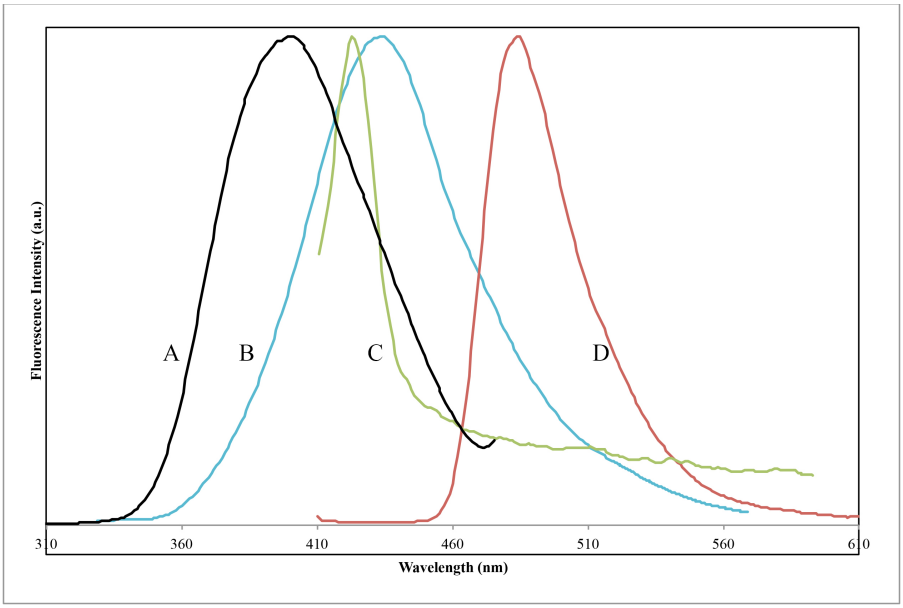

Figure 16. Emission spectra of A) tris(5-chloro-8-hydroxyquinolinato)bismuth (**1**),with an excitation wavelength of 330 nm; B) triethylammonium tris(7-iodo-8-hydroxyquinolinato-5-sulfonate)bismuthate (**9**) with an excitation wavelength of 352 nm; C) tris(2-(diethoxymethyl)-8-quinolinato)bismuth (**6**),with an excitation wavelength of 260 nm; D, tris(8-hydroxy-5-nitroquinolinato)bismuth (**8**), with an excitation wavelength of 309 nm. Spectrum C was taken in CH_2Cl_2 at 298K. Spectra A, B and D were taken in DMF at 298 K

The emission spectra (Figure **15**) of compounds **2, 3, 4, 5,** and **7** all show dual emission in solution. The higher energy emission feature is sharper and falls between 370 – 400 nm for the three compounds. The lower energy maxima peak is broader and falls between 520 – 550 nm. This band is broad with a full width half maximum 83, 78, 82, and 87 nm, respectively.

The lower energy emission features in compounds **3** and **7** are blue-shifted from Biq_3 by 20 and 15 nm, but remain in the green region of the spectrum. It can be assigned to the lowest π-π* transition on the ligand similar to that seen previously in both Alq_3 and Biq_3. For compounds **4** and **5**, the lower energy emission features are blue-shifted by 8 and 20 nm, respectively, from the Biq_3 emission band. X-ray structural analysis shows that both complexes are dimeric with the bismuth metals connected to each other via Bi_1-O_B bonds between monomers.

The emission spectra (Figure **16**) for tris(5-chloro-8-hydroxyquinolinato)bismuth (**1**), tris(2-(diethoxymethyl)-8-quinolinato)bismuth (**6**), triethylammonium tris(7-iodo-8-hydroxyquinolinato-5-sulfonate)bismuthate (**9**), and tris(8-hydroxy-5-nitroquinolinato)bismuth **(8)** were collected at room temperature. These four compounds exhibit emission spectra significantly blue-shifted from Biq_3. All the compounds exhibit a single emission peak in the range of 400-500 nm. Compound **6** has a much narrower emission band shape than the others.

The largely blue-shifted emission peaks of compounds **1, 6, 8,** and **9** may result from a decreased tendency to dimerize. The long Bi-N bonds in the monomer structure indicates decreased covalent bonding between the hydroxyquinolate nitrogen and the metal center, which is known to result in a large blue shift of the lowest energy π-π*

(phenoxide→ pyridyl) transition of the quinolate ring.[5,33,34] The molecular structures of the monomeric bismuth(III) compound shows a facial geometry with the nitrogen atoms of the quinolate ring surrounding the region of the stereochemically active lone pair on bismuth. This leads to an unusually long Bi-N bond length in comparison to those found in the dimeric structures and may account for the blue shifted emission band. The dual emission observed can be attributed to simultaneous emission by monomeric (short wavelength emission) and dimeric species (long wavelength emission) present in solution.

Compound **8** emits in the 480 nm region, while compounds **6** and **9** emit near 430 nm. The HOMOs for these three compounds are localized on the phenoxide ring, while the the LUMOs are more localized on the pyridyl ring.[35] Due to their electron withdrawing properties, all three substituents (NO_2, SO_3^- and $-C(OEt)_2$) will affect the distribution of π electron density of 8-hydroxyquinoline. Adding an EWG to the 5-position will lower the HOMO- LUMO energy with respect to Biq_3. The inductive influence and resonance capabilities of NO_2 and SO_3^- also can act to stabilize the HOMO, thereby increasing the energy gap and promoting a blue shift in emission.[35] Delocalization of electrons from the phenoxide ring is also extended to the NO_2 or SO_3^- and can alter the energy of the n-π* transitions, causing a further increase in energy for this transition.[36] Table **15** gives the photophysical data for all the compounds.

Table 15. Photoluminescent properties of compounds **1-9** in solution at room temperature.

	UV (nm) (ε), compound	UV (nm) (ε), ligand	Emission λ_{max}, (nm) (λ_{excit}, nm)	Φ_F	Conditions
1	246 (86,654), 330 (10101)	245.82 (42871), 329.95 (4875)	423 (330)	<0.001	DMF, 298K
2	233(11812), 271(20546), 346(4172), 408 (5090)	267.1(1055.2), 320.46 (1178.6)	525 (350)	0.0013	DMF, 298K
3	254(111862), 353(11865), 418 (14832)	265.93(4300), 355.49 (690.8)	371, 520 (354)	0.003	DMF, 298K
4	274(65742), 350(11668), 412 (11726)	271.35(2702), 324.32 (1623)	393, 542 (352)	<0.001	DMF, 298K
5	246(25450), 307(1835), 385 (842)	246.98 (45306), 303.83(2318)	390, 526 (354)	<0.001	DMF, 298K
6	253(7217), 400 (597)	264.39(54740), 306.92 (3825), 371.89 (2551)	433 (380)	0.001	CH_2Cl_2, 298K
7	234(42747), 271(49667), 324(20562), 402 (5497)	265.14 (3687)	388, 526 (346)	0.006	DMF, 298K
8	265(36718), 348(14392), 447 (82108)	264.9 (3481), 357.55 (1452), 460.25 (15)	484 (309)	0.001	DMF, 298K
9	273(15800), 336(9178), 379 (11524)	265.55 (3451), 316.07 (1222)	430 (351)	0.094	DMF, 298K

4.2 *Emission Spectra at Varying Concentrations*

Emission spectra were taken for tris(5,7-dichloro-8-hydroxyquinolinato)bismuth (Compound **2**), bis(μ_2-5-chloro-7-iodo-8-hydroxyquinolinato)tetra(5-chloro-7-iodo-8-hydroxyquinolinato)dibismuthine (**4**), bis(μ_2-7-bromo-8-hydroxyquinolinato)tetra(7-bromo-8-hydroxyquinolinato)dibismuthine 2-tetrahydrofuran (**5**), and tris(2-(diethoxymethyl)-8-quinolinato)bismuth (**6**) at various concentrations to observe if oligomerization at higher concentrations influenced the emission spectra. All compounds were first dried under vacuum for 24-48 h and dissolved in CH_2Cl_2. The spectra were all taken at room temperature.

The emission spectra of compound **2** (Figure **17**) was further studied for the effect of dimerization with increasing concentration. The emission spectra were taken in CH_2Cl_2 at 298K with an excitation wavelength of 401 nm. Figure **17** shows that compound **2** produces mostly one broad emission band at 526 nm at higher concentration and predominantly one emission band at 440 nm at lower concentrations. Because dimerization occurs at higher concentrations, the dimer form of compound **2** can be assigned to the lower energy emission peak while the monomer is assigned the higher energy emission peak.

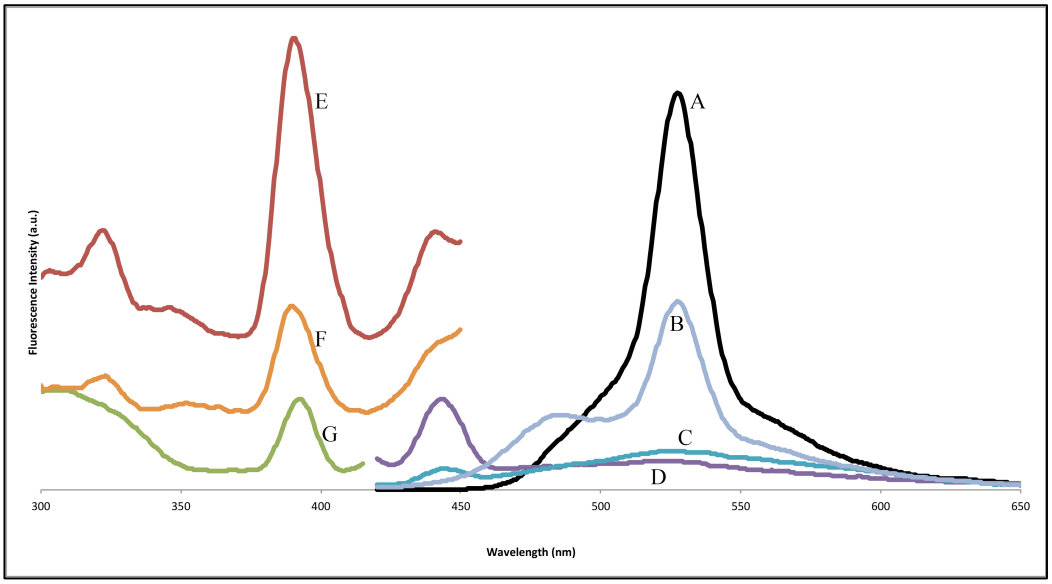

Figure 17. Excitation and emission spectra of tris(5,7-dichloro-8-hydroxyquinolinato)bismuth (Compound **2**) at varying concentrations. A/E: [**2**] = 8.23 x 10^{-4} M, B/F: [**2**] = 2.75 x 10^{-4} M, C: [**2**] = 7.35 x 10^{-5} M, D/G: [**2**] = 1.62 x 10^{-5} M. Emission spectra were taken in CH_2Cl_2 at 298K with an excitation wavelength of 401 nm. Excitations spectra E and F were observed at an emission wavelength of 526 nm while excitation spectra G had an emission wavelength of 440 nm.

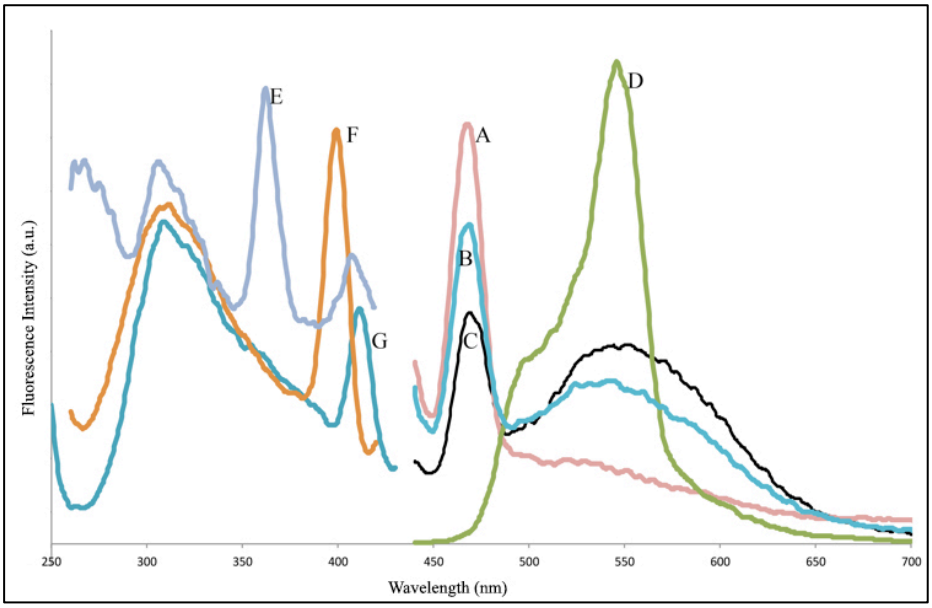

Figure 18. Excitation and emission spectra of bis(μ_2-5-chloro-7-iodo-8-hydroxyquinolinato)tetra(5-chloro-7-iodo-8-hydroxyquinolinato)dibismuthine (Compound **4**) at varying concentrations. A/F: [**4**] = 6.29 x 10^{-6} M, B: [**4**] = 1.53 x 10^{-5} M, C/G: [**4**] = 2.92 x 10^{-5} M, D/E: [**4**] = 3.21 x 10^{-4} M. Emission spectra were taken in CH_2Cl_2 at 298K with an excitation wavelength of 408 nm. Excitation spectrum E had an emission wavelength of 534 nm, while excitation peaks F and G had an emission wavelength of 460 nm.

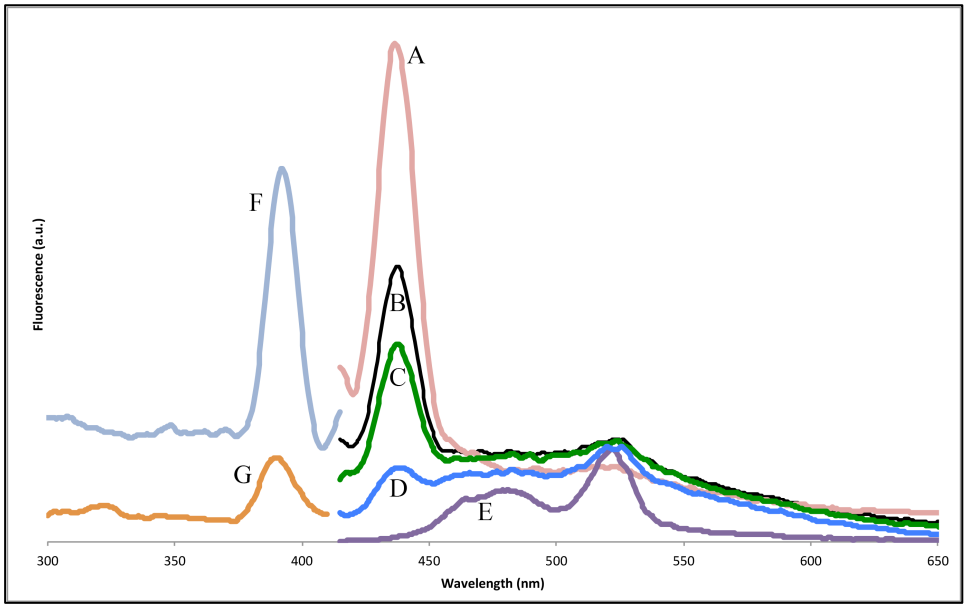

Figure 19. Excitation and emission spectra of bis(μ_2-7-bromo-8-hydroxyquinolinato)tetra(7-bromo-8-hydroxyquinolinato)dibismuthine 2-tetrahydrofuran (Compound **5**) at varying concentrations. A/F: [**5**] = 6.92 x 10^{-6} M, B: [**5**] = 3.21 x 10^{-5} M, C: [**5**] = 4.60 x 10^{-5} M, D: [**5**] = 8.83 x 10^{-5} M, E/G: [**5**] = 3.53 x 10^{-4} M. Emission spectra were taken in CH_2Cl_2 at 298K with excitation at 385 nm. Excitation spectrum G was monitored at an emission wavelength of 520nm, while excitation peak F used an emission wavelength of 440 nm.

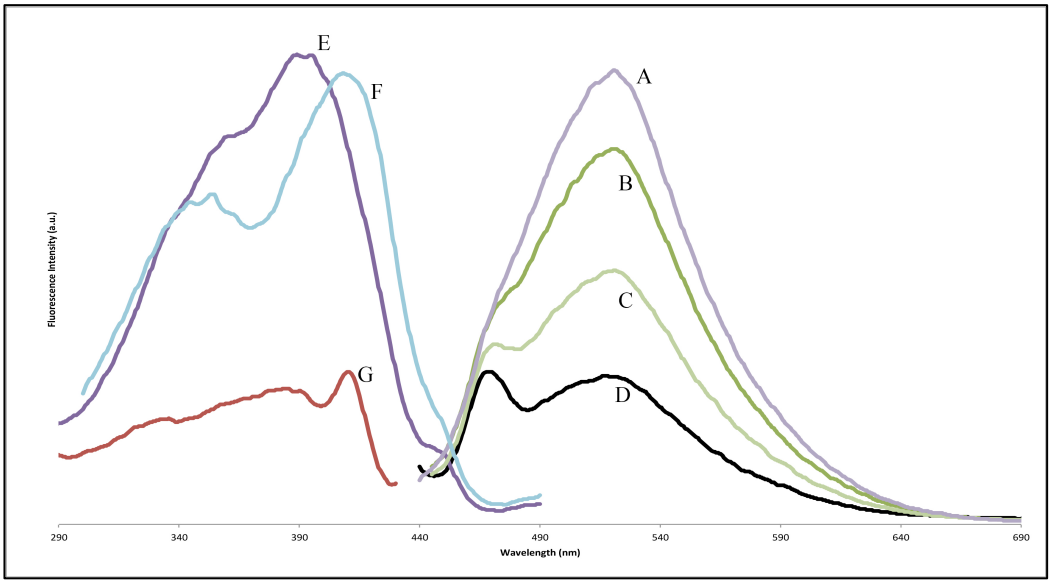

Figure 20. Excitation and emission spectra of tris(2-(diethoxymethyl)-8-quinolinato)bismuth (Compound **6**) at varying concentrations and degrees of dimerization. A/F: [**6**] = 1.61 x 10^{-4} M, B/E: [**6**] = 8.42 x 10^{-5} M, C: [**6**] = 6.80 x 10^{-5} M, D/G: [**6**] = 3.47 x 10^{-5} M. Emission spectra were taken in CH_2Cl_2 at 298K with an excitation wavelength of 391 nm. Excitation spectra E and F monitored an emission wavelength at 518 nm while excitation spectrum G used an emission wavelength at 497 nm.

The emission spectra at high (3.21×10^{-4} M) and low (6.29×10^{-6} M) concentrations for compound **4** (Figure **18**) show that as the concentration increases, the emission spectra show the formation of a new peak (534 nm), which is consistent with long wavelength from the dimer form. The emission peak at 460 nm starts to decrease with increasing concentration, while the lower energy peak increases in intensity proportionally to concentration. Figure **19** shows the emission spectra at varying concentrations for bis(μ_2-7-bromo-8-hydroxyquinolinato)tetra(7-bromo-8-hydroxyquinolinato)dibismuthine 2-tetrahydrofuran (**5**). At lower concentrations (6.92×10^{-6} M), there is a prominent peak at around 440 nm; at higher concentration (3.53×10^{-4} M), there is a more prominent emission peak at 520 nm. The spectra suggest that the compound has a higher energy transition in the monomeric form than as a dimer.

In Figure **20**, the emission spectra at varying concentrations for tris(2-(diethoxymethyl)-8-quinolinato)bismuth (**6**) are shown. At lower concentrations, compound **6** exhibits a broad peak at 518 nm and another emission band at 467. Like the previous compounds, at higher concentrations, the higher energy peak corresponding to the monomer decreases. The monomer peak in this complex is red shifted compared to the monomer peaks in other compounds. This could be due to the position of the substitutent on the pyridyl. In the monomer form, there is very little π-stacking because of the distorted octahedral geometry. The acetal positions are sterically hindered and would be unfavorable to be in the 2-position in the geometry seen in the dimers.

Like boron quinolate complexes, the blue shift in emission observed between the monomeric to dimeric forms can be attributed to the weak bismuth to nitrogen bond character.[33] Chen and Shi determined that decreasing covalent character in the metal-nitrogen bond results in a blue shift of the lowest quinolate electronic transitions.[5] Not only does bismuth have more ionic metal-ligand bonding character, but the longer Bi-N bond lengths observed in complexes **4, 5, 6,** and **9** were verified by the X-ray diffraction analysis. When the bond length between metal and nitrogen are decreased, emission tends to shift to a higher energy wavelength.[5,33,34]

Emission spectra were observed for these four compounds in degassed CH_2Cl_2 at high and low concentrations at 298K. The compounds were first dried under vacuum and then dissolved in solution. The emission spectra were taken for these compounds at recorded concentrations. These solutions were then degassed with argon for 20 minutes. The color of the solutions did not change. The degassed emission spectra did not show a quenching of the emission peaks, indicating that dioxygen does not quench the emission in these compounds.

Chapter 5

Electronic Structure Calculations

5.1 *Overview*

To obtain a better understanding of the electronic structures of the mononuclear and dinuclear structures found in the crystalline compounds **4, 5, 6** and **9,** density functional theory (DFT) calculations were employed.

Qualitatively, in the monomer, the uppermost occupied orbitals are three π bonding orbitals localized on the phenoxide ring. The LUMO orbitals contain the three corresponding antibonding orbitals that are more localized on the pyridyl ring. In the dimer, the antibonding and bonding π orbitals are split and doubled due to the fact that there are twice as many ligands. However the six upper occupied orbitals are still π orbitals localized on the phenoxide while the six lowest empty orbitals in the dimer are π* orbitals localized on the pyridyl ring. The face-to-face overlap of two pairs of quinolate rings in the dimer reduces the HOMO-LUMO π-π* gap. In the dimers, the face-to-face π interaction should cause the repulsed, filled orbitals to be raised in energy. The uppermost orbitals in the dimers are predominantly the equatorial pi systems and their destabilizationcauses a decrease in the HOMO-LUMO gap. In addition, excited state coupling effects, such as exciton splitting, would further shift and split the ligand localized π-π* transition.

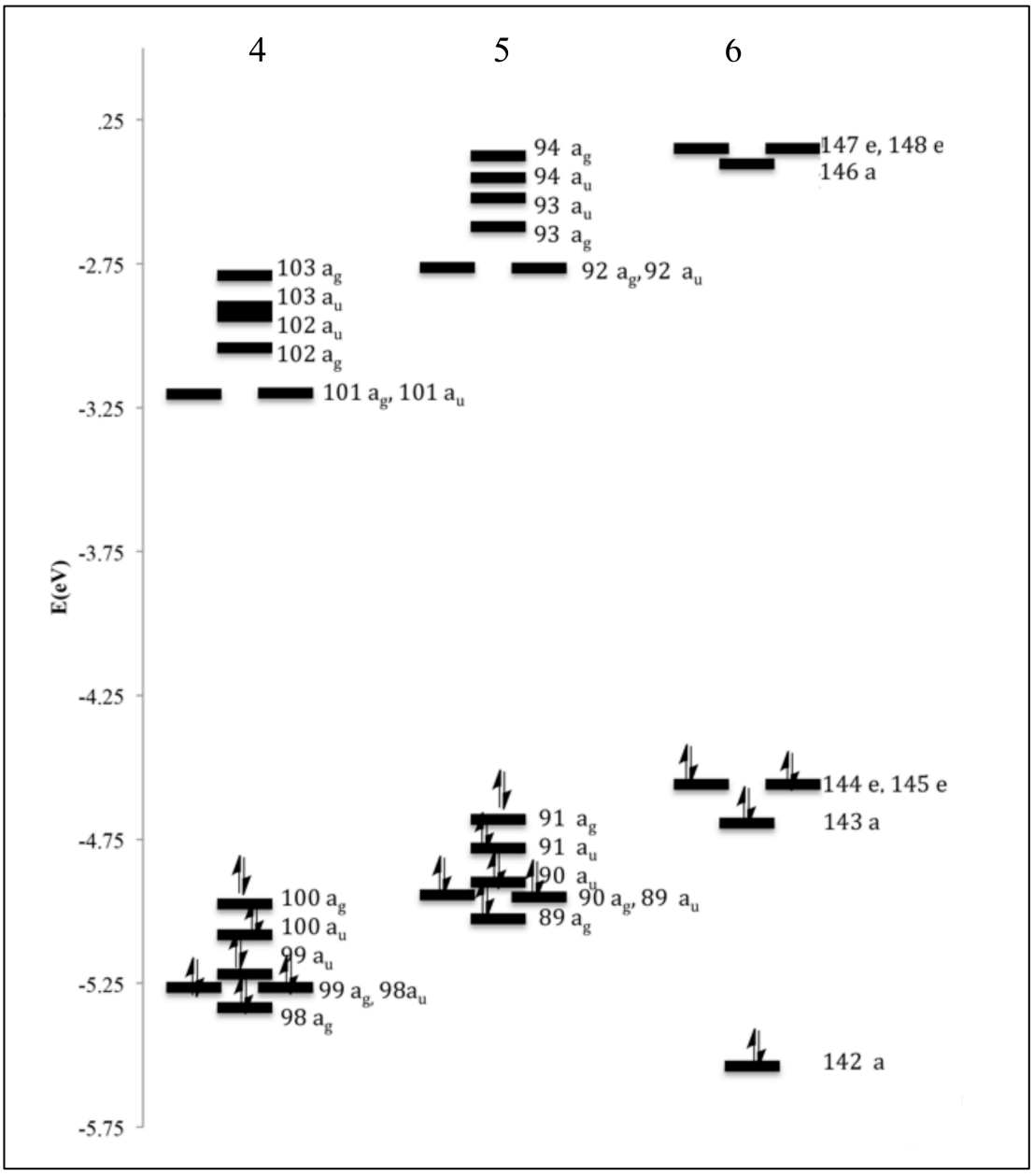

Figure 21. Energy Level Diagram of Frontier Quinolate π Orbitals of Compounds **4, 5,** and **6.**

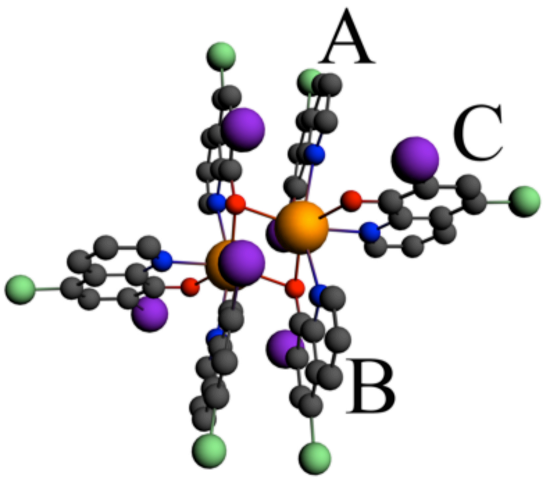

Figure 22. Ligands labeled for clarity in compound **4.**

Table 16. Molecular orbital compositions (percentage) of frontier orbitals in compound **4.**

	Bi	**I'**	**Cl'**	**O_A**	**N_A**	**O_B**	**N_B**	**O_C**	**N_C**
103 a_g				1.27	8.99	1.5	8.89		
103 a_u	7.66			1.42	8.38	1.52	7.48		1
102 a_u	1.69				9.02		9.8		
102 a_g	2.02				7.19		8.94		
101 a_g	1.66				1.17			2.2	13.92
101 a_u	1.18							2.12	15.37
100 a_g		10.08	6.58	9.19		12.05			
100 a_u		10.04	7.14	9.82		8.7			
99 a_u		5.74	7.44	8.74		9.18	1.28		
99 a_g		9.25	7.46					19.62	1.75
98 a_u		9.26	7.45					20.23	1.71
98 a_g	1.23	5.83	8.27	7.33	1.38	7.14	1.22	1.86	1.22

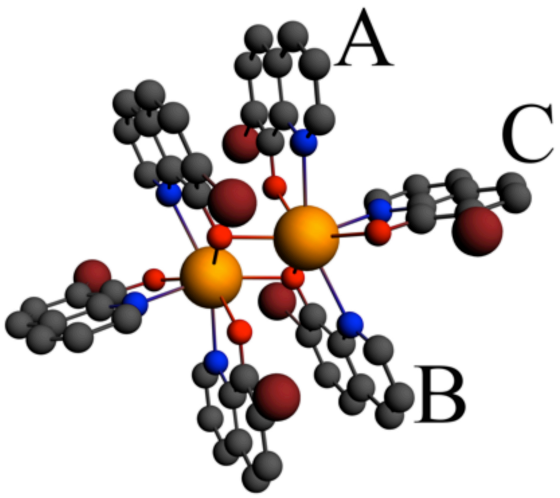

Figure 23. Ligands labeled for clarity in compound **5.**

Table 17. Molecular orbital compositions (percentage) of frontier orbitals in compound **5.**

	Bi	**Br**	**O_A**	**N_A**	**O_B**	**N_B**	**O_C**	**N_C**
94 a_g				9.54		9.78		
94 a_u	4.4			18.35				
93 a_u	5.19					16.93		1.23
93 a_g	6.61			8.07		9.12		
92 a_g							2.14	16.26
92 a_u							2.09	16.09
91 a_g		8.05	10.02		15.6			
91 a_u		7.68	7.78		16.12	1.05		
90 a_u		4.56	13.32	1.18	3.4		4.09	
90 a_g		8.41					22.75	1.02
89 a_u		7.23					19.23	
89 a_g	1.36	6.01	11.17	1.55	6.21		1.85	

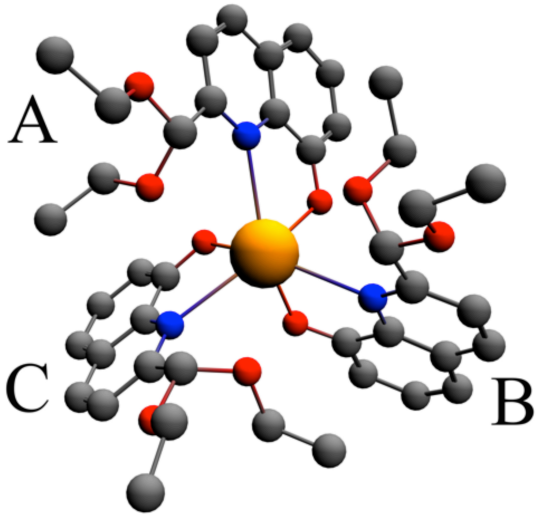

Figure 24. Ligands labeled for clarity in compound **6**.

Table 18. Molecular orbital compositions (percentage) of frontier orbitals in compound **6.**

	Bi	**O_A**	**N_A**
147 e	1.95	1.09	19.83
148 e	1.95	1.11	20.97
146 a	5.16		20.00
145 e		26.17	
144 e		25.46	
143 a	1.28	22.24	
142 a	11.96	35.60	21.09

The molecular orbital compositions for each energy level are given in Tables **16-18** for compounds **4, 5,** and **6** for the heteroatom components of the frontier orbitals that are predominantly associated with the hydroxyquinolate π system. Compounds **4** and **5** were calculated with idealized C_i symmetry, while compound **6** was calculated with an idealized C_3 geometry. The bismuth metal centers have only a minor contribution to the frontier orbitals in these compounds.

X-ray diffraction analysis has shown that compounds **4** and **5** are dimers, with two of the quinolate ligands (L_A and L_B) from each molecule in a pseudo equatorial postion parallel to the each other (Figure **22** and **23**). The planes of these two ligands face each other in the dimer structure creating a π interaction. The final quinolate ligand (L_C) is pseudoaxial and lies perpendicular to ligands L_A and L_B. Ligand L_c, under density functional theory (DFT) analysis, contributes little to the HOMO/LUMO orbitals in the dimers. The calculated HOMO-LUMO energy gap in compound **4** is 1.772 eV (700 nm) and in compound **5** it is 1.915 eV (647 nm), which is reduced from the value found in the monomer **6** at 2.156 eV (575 nm). The decreased energy correlates with observed trends in the experimental emission and absorption peaks that had lower energy bands appear at higher concentrations. The Bi-Bi bond distance is 3.604Å for compound **4** and 3.674Å for compound **5**.

For ligands L_A and L_B in the dimers, the HOMO electron cloud is mostly π character (Table **16** and **17**) and concentrated on the phenoxide rings. Similarly, the electron clouds of the LUMO are concentrated on the nitrogen and carbon atoms of the pyridyl ring and are mostly composed of π character (Figure **25-28**).

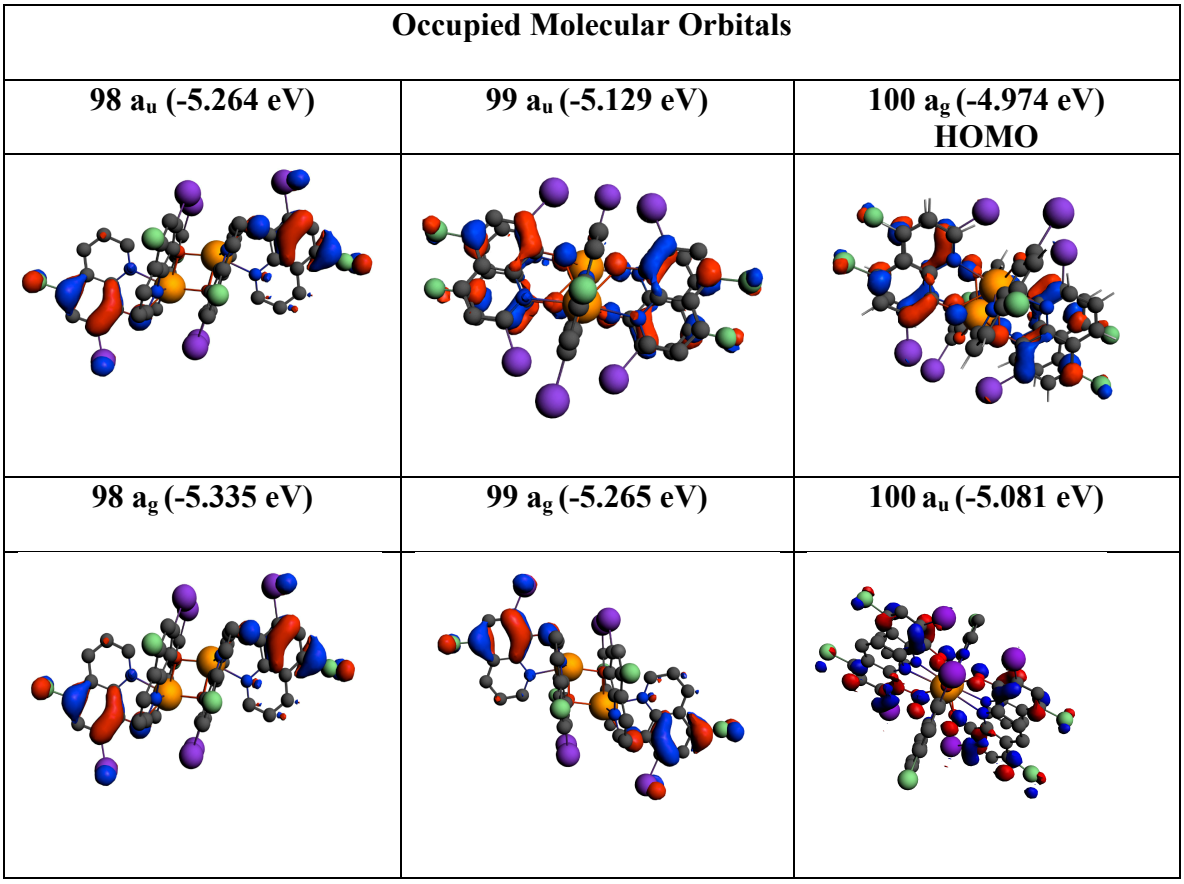

Figure 25. Occupied molecular orbitals for compound **4.**

Unoccupied Molecular Orbitals		
101 a_g (-3.202 eV) LUMO	**102 a_u (-2.933 eV)**	**103 a_g (-2.971 eV)**
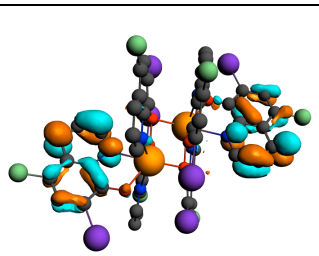	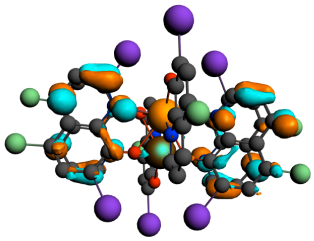	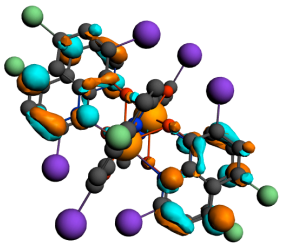
101 a_u (-3.198 eV) LUMO	**102 a_g (-3.042 eV)**	**103 a_u (-2.898 eV)**
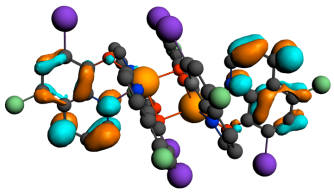	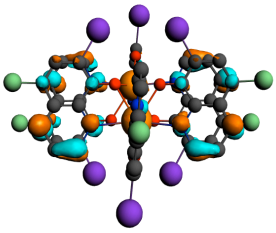	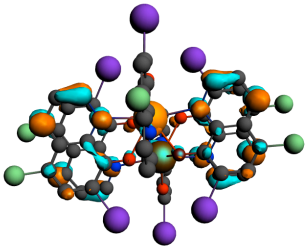

Figure 26. Unoccupied molecular orbitals for compound **4.**

Occupied Molecular Orbitals		
89 a_g (-5.027 eV)	**90 a_g (-4.943 eV)**	**91 a_g (-4.680 eV) HOMO**
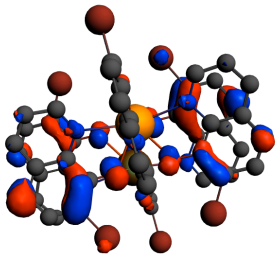	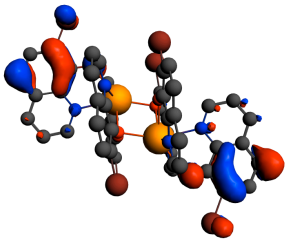	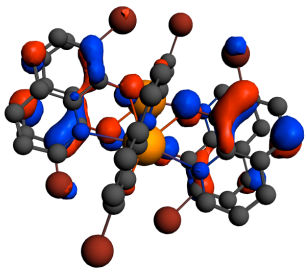
89 a_u (-4.950 eV)	**90 a_u (-4.899 eV)**	**91 a_u (-4.780 ev)**
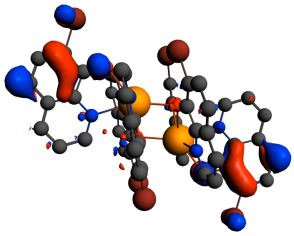	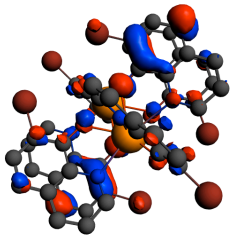	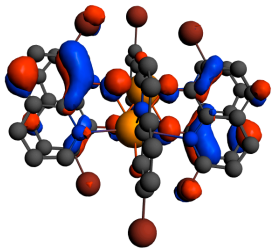

Figure 27. Occupied molecular orbitals for compound **5.**

Unoccupied Molecular Orbitals		
92 a_g (-2.763 eV) LUMO	**93 a_g (-2.620 eV)**	**94 a_g (-2.374 eV)**
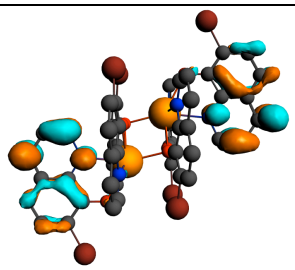	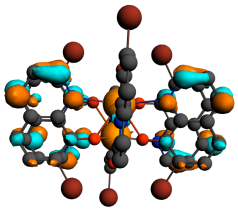	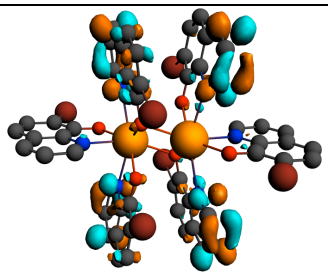
92 a_u (-2.765 eV) LUMO	**93 a_u (-2.520 eV)**	**94 a_u (-2.451 eV)**
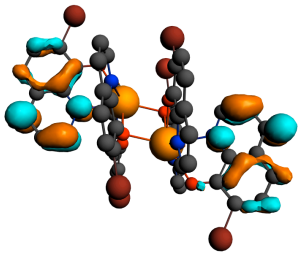	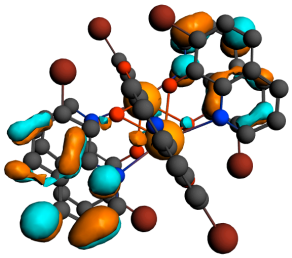	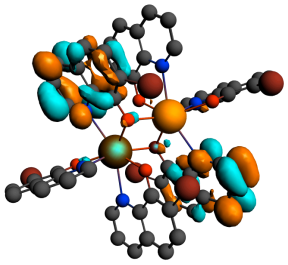

Figure 28. Unoccupied molecular orbitals for compound **5**.

Occupied Molecular Orbitals	
142 a (-5.537 eV)	**143 a (-4.694 eV)**
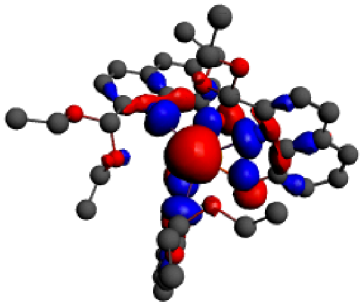	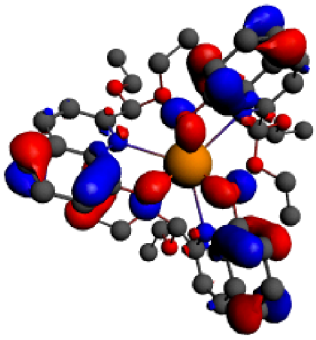
144 e (-4.559 eV) **HOMO**	**145 e (-4.558 eV)** **HOMO**
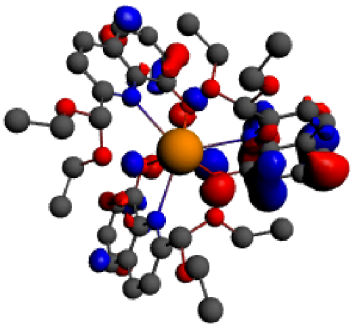	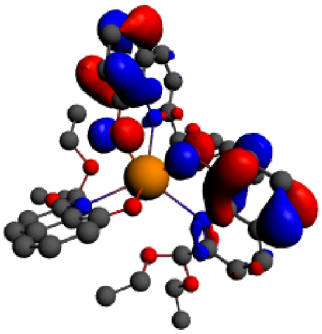

Figure 29. Occupied molecular orbitals for compound **6.**

Unoccupied Molecular Orbitals		
146 a (-2.403 eV) LUMO	**147 e (-2.349 eV)**	**148 e (-2.348 eV)**
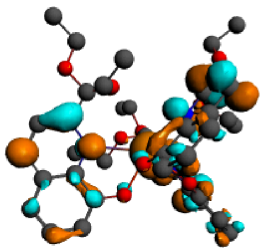	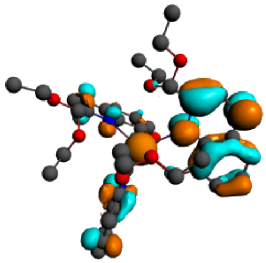	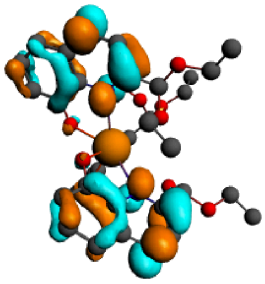

Figure 30. Unoccupied molecular orbitals for compound **6**.

Compound **6** was shown to be a monomer in the solid state with a distorted octahedral geometry. Because of the compounds *fac* isomer preference, DFT analysis was calculated with an idealized C_3 symmetry. In this compound, the HOMO and LUMO levels are also mainly ligand-localized with the HOMO level concentrated on the phenoxide ring and the LUMO level concentrated on the pyridyl ring of the quinolate (Table **18,** Figure **29** and **30**). The calculated HOMO-LUMO energy gap is 2.156 eV (575 nm) is higher than in the dimeric compounds. The bismuth metal center is again a minor contributor to frontier orbitals.

Like compounds **4** and **5**, the electron clouds of the occupied frontier π orbitals are concentrated on the phenoxide ring, with predominant π character. The LUMO is of π character concentrated on the pyridyl ring.

The molecular orbital energy diagram for compound **9** is given in Figure **31**. In compound **9**, the sulfonate anion was neutralized with a bound proton in the calculation. The compound was calculated without a net charge and idealized with C_s symmetry. The ligand arrangement is similar to that of the dimeric compounds **4** and **5** but without a bridging ligand. The bismuth center also contributes minimally to the frontier orbitals of this compound.

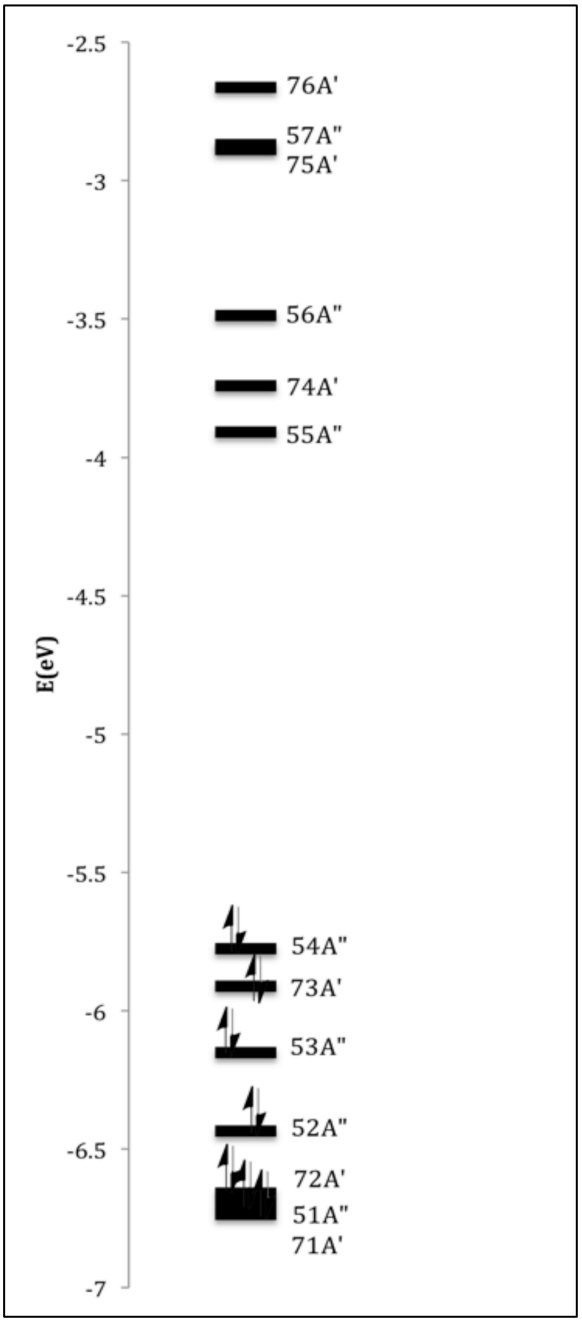

Figure 31. Energy Level Diagram of the Frontier Quinolate π Orbitals of Compound **9** computed with the use of density functional theory**.**

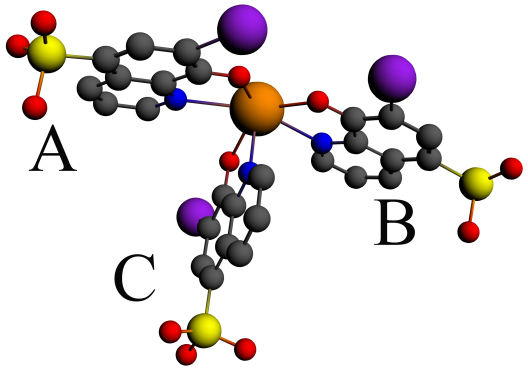

Figure 32. Ligands labeled for clarity in compound **9**.

Table 19. Molecular orbital compositions (percentage) of frontier orbitals in compound **9**.

	Bi	**$O_{A/B}$**	**$N_{A/B}$**	**O_C**	**N_C**
76 a'	3.15				
57 a"					
75 a"	49.53	5.86	4.92	1.1	6.53
56 a"		3.31	16.56		
74 a'	18.97	1.12	11.77		4.19
55 a"	1.85			3.17	14.7
54 a"		17.98	1.72		
73 a'		14.79	2.07		
53 a"			20.09	4.85	1.99
52 a"		2.32			
72 a'	1.16	7.59			
51 a"		3.95			
71 a'		4.76			

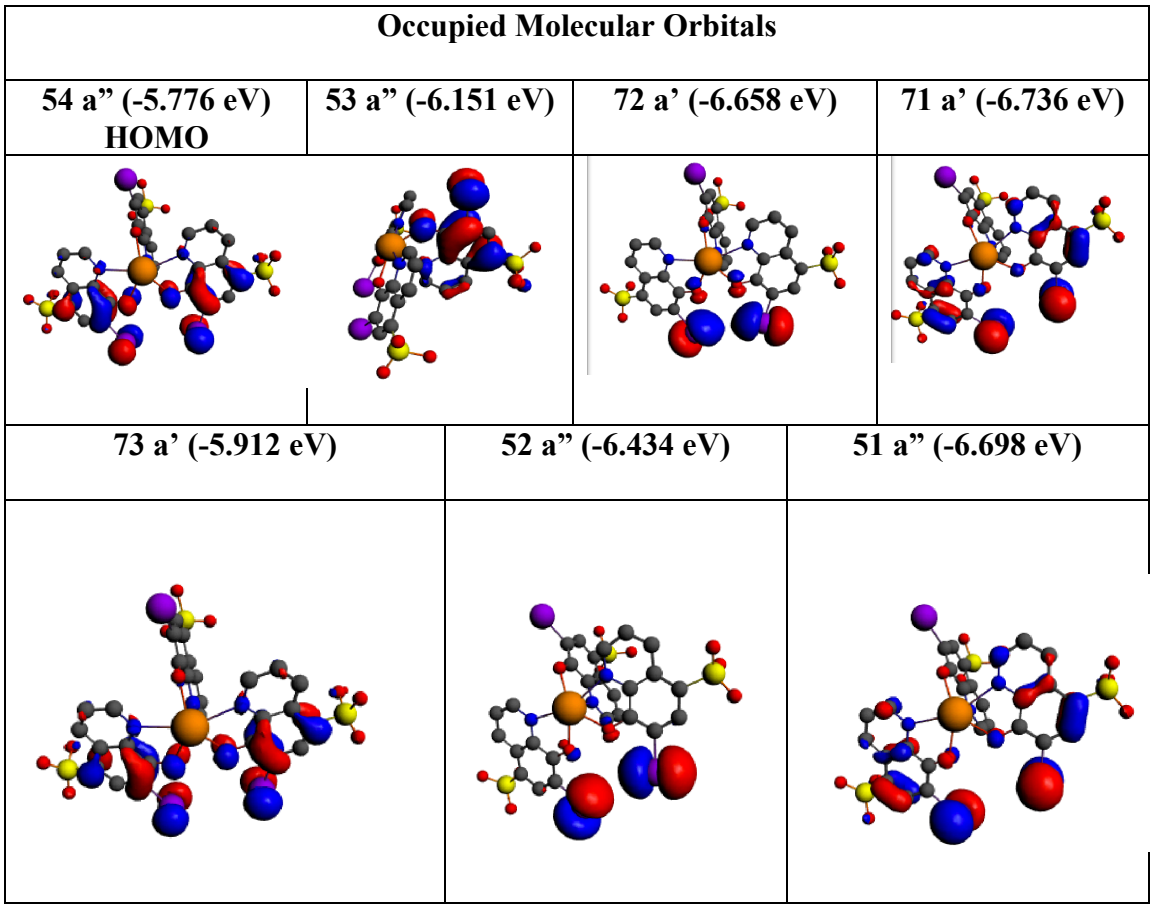

Figure 33. Occupied molecular orbitals for compound **9.**

Unoccupied Molecular Orbitals		
57 a" (-2.870 eV)	**56 a" (-3.488 eV)**	**55 a" (-3.908 eV) LUMO**
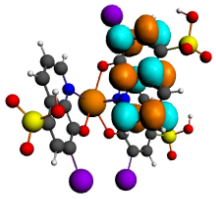		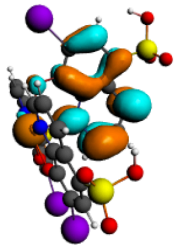
76 a' (-2.664 eV)	**75 a' (-2.888 eV)**	**74 a' (-3.742 eV)**
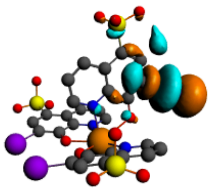	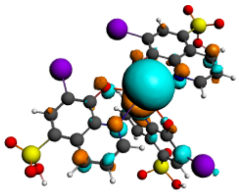	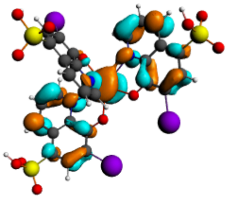

Figure 34. Unoccupied molecular orbitals for compound **9.**

The frontier orbitals of compound **9 (**Figures **33** and **34**) are also ligand localized with a calculated HOMO-LUMO gap of 1.868 eV (664 nm). The HOMO is chiefly composed of phenoxide ring character from L_A and L_B. This is similar to that of dimers **4** and **5**, which have a similar arrangement of the quinolate ligands about the metal center.

In general, the uppermost occupied orbitals of the monomeric and dimeric complexes are primarily π in character and localized on the phenoxide ring. The lowest unoccupied orbitals are located on the pyridyl ring and are π^* in character. The face-to-face orientation of the two pairs of quinolate ligands in the dimeric structures results in a decreased HOMO-LUMO gap that is reinforced by an exciplex-like interaction in the lowest excited state. The solution UV-vis studies show an equilibration between monomeric and dimeric forms for most BiL_3 compounds and that the dimeric form possesses lower energy absorptions than the corresponding monomer.

Chapter 6

Conclusions

Nine substituted 8-hydroxyquinolates of bismuth(III) were prepared and found that they could adopt either monomeric structures or hydroxyquinolate oxygen bridged dimeric structures. Dimer formation tended to form in compounds that had 8-quinolinols substituted with less steric bulk. Monomer formation occurred in compounds with more hindered substituents. Additionally, the Bi(III) monomer preferred a facial orientation that is different from the meridional isomer favored for Al(III) and Ga(III) quinolinol complexes. The dimeric structures appear to also be favored by a donor-acceptor p-stacking interaction between the quinolate ligands on adjacent Bi(III) so that the penoxide ring of one quinolate likes above the pyridyl ring of the adjacent quinolate.

UV-Vis Absorption spectra and emission spectra both showed a blue shift of the absorption spectra in these compounds from the non-substituted Biq_3 and Alq_3. This is most likely due to the decreasing covalent nature of the bismuth-nitrogen bond because of substituent electronic effects on the 8-hydroxyquinolate ligand and/or stereochemically bulky substituents on the pyridyl ring. Looking at the monomer-dimer equilibrium dynamics with the help of UV-Vis spectroscopy demonstrated that at high concentration, all compounds exhibited a tendency to form dimers. The compounds that crystallized out as dimers had the highest K for dimer formation, while the compounds with the smaller K values were isolated as monomers.

Fluorescence spectroscopy demonstrated that most compounds have dual emission peaks in solution at varying concentrations that wer attributable to the monomer-dimer equilibrium. Dimer emission peaks emerged at lower energies when

the solution concentration was increased. In electronic structure calculations, the monomers had the three uppermost π-bonding orbitals localized on the phenoxide ring while the three lowermost unoccupied orbitals were localized on the pyridyl ring. The dimers demonstrated a doubling of these frontier π orbitals that were seen in the monomer. Additionally, the face-to-face overlap of quinolate rings in the dimers reduce the HOMO-LUMO π-π* gap and explain the lowered energy of emission in the dimers.

The placement of the monomer and dimer peaks correlate with trends in the calculated HOMO-LUMO energy gap. There is an increased energy gap in the monomer form of the complex when compared to the calculated dimer HOMO-LUMO energy gap, thus giving rise to the emission band at the shorter wavelength in the monomer. The solid-state emission spectra further support the idea of an increased energy for the lowest absorption in the monomer. Compound **6** is sterically hindered from π –stacking interactions preventing solid state dimerization.. The solid-state emission spectrum of this compound, does not have a longer wavelength solid-state emission peak.

More research needs to be done in the tuning of the substituents on the 8-hydroxyquinolate groups. The π-π* transfer from the phenoxide ring to the pyridyl ring on the quinolinol makes these ligands a very interesting coordination complex when paired with a heavy atom such as bismuth.

Chapter 7

Materials and Methods

7.1 *General Methods*

The 5-chloro-8-hydroxyquinoline ligand was purchased from Alfa Aesar. 5-Chloro-8-hydroxy-7-iodoquinoline and 7-iodo-8-hydroxyquinoline-5-sulfonic acid were purchased from TCI America. 5,7-Dichloro-8-hydroxyquinoline, 5,7-diiodo-8-hydroxyquinoline, 8-hydroxy-5-nitroquinoline, 7-bromo-8-hydroxyquinoline, and bismuth (III) chloride were purchased from Sigma-Aldrich. 8-Hydroxyquinoline-2-carboxylic acid and 8-hydroxyquinoline-2-carboxaldehyde were purchased from Acros Organics Dry THF was purchased from Aldrich Chemical Co. Inc. and used after purification with an MBraun MB Auto Solvent Purification System using a dry nitrogen atmosphere. Spectroscopic grade dichloromethane (CH_2Cl_2) and *N,N'*-dimethylformamide (DMF) were purchased from Aldrich Chemical Co. and used for spectroscopic measurements. All other reagents were purchased from Aldrich Chemical Co. and used as received. Synthetic procedures were carried out under a dry argon gas atmosphere using standard Schlenk techniques.

Elemental combustion analyses were performed by Numega Resonance Labs, Inc. for C, H, and N. Fluorescence emission and excitation spectra were recorded with the use of a Perkin-Elmer Luminescence Spectrometer LS-50. UV-spectra were obtained with the use of a Perkin-Elmer Lambda 35 UV/Vis spectrometer. NMR data was collected with the use of either a JEOL 500MHz spectrometer or a Varian 400 MHz spectrometer and analyzed with JEOL Delta software. All measurements were taken at ambient temperature.

Tris(5-chloro-8-hydroxyquinolinato)bismuth **(1)**. Bismuth (III) chloride (0.50g, 1.60 mmol) was dissolved in dry ethanol (60.0 mL) in a round bottom flask under argon at room temperature and stirred. After the bismuth (III) chloride dissolved into a clear solution, 5-chloro-8-hydroxyquinoline (0.85g, 4.8 mmol) was added to the stirring mixture. The reaction was refluxed at 343 K for 3 h under an argon atmosphere. The reaction turned a dark yellow and was cooled to room temperature. Triethylamine and deionized water (10mL) were added to neutralize the HCl produced, and a light yellow precipitate formed that was vacuum filtered and washed with ethanol (2 x 30mL), deionized water (2 x 30mL), and diethyl ether (2 x 30mL). The compound was vacuum-dried and recrystallized by dissolving it in warm THF (323K), filtering, cooling to room temperature and drying under vacuum. This process was repeated once more and yielded a bright yellow colored powder (1.085 g, 92%). Anal. Calcd. for $C_{27}H_{15}BiCl_3N_3O_3$: C, 43.54: H, 2.03: N, 5.64. Found: C, 43.05: H, 2.03: N, 6.5.

Tris(5,7-dichloro-8-hydroxyquinolinato)bismuth **(2).** Compound **2** was obtained in a similar manner as compound **1** from bismuth (III) chloride (0.473 g, 1.5 mmol) and 5,7-dichloro-8-hydroxyquinoline (0.963 g, 4.5 mmol) in ethanol (60 mL). Triethylamine and deionized water (10 mL) were added to neutralize the HCl produced, and precipitate the crude compound. Compound **2** was recrystallized from warm THF (323K) and cooled to room temperature. The purification process was performed twice and yielded a yellow-orange powder that was dried under vacuum

(1.165 g, 92%). Anal. Calcd. for $C_{27}H_{12}BiCl_6N_3O_3$: C, 38.24: H, 1.43: N, 4.95. Found: C, 38.21: H, 1.43: N, 4.88.

Tris(5,7-diiodo-8-hydroxyquinolinato)bismuth (**3***)*. Compound **3** was prepared in a similar manner as compound **1** from bismuth (III) chloride (0.315 g, 1 mmol) and 5,7-diiodo-8-hydroxyquinoline (1.19 g, 3 mmol) in ethanol (60 mL). Triethylamine and deionized water (10 mL) were added to neutralize the HCl produced, and precipitate crude compound. The compound was recrystallized from warm THF (323K) and precipitated by cooling to room temperature to yield a dark orange crystalline powder (1.24 g, 89%). Anal. Calcd. for $C_{27}H_{12}BiI_6N_3O_3$: C, 23.22: H, 0.87: N, 3.01. Found: C, 23.13: H, 1.02: N, 3.22.

*Bis(μ_2-5-chloro-7-iodo-8-hydroxyquinolinato)tetra(5-chloro-7-iodo-8-hydroxyquinolinato)dibismuthine (***4***)*. Compound **4** was prepared in a similar manner as compound **1** from bismuth (III) chloride (0.315 g, 1 mmol) and 5-chloro,7-iodo, \8-hydroxyquinoline (0.916 g, 3 mmol) in ethanol (60 mL). Triethylamine and deionized water (10 mL) were added to neutralize the HCl produced, and precipitate crude compound. The crude powder was dried under vacuum. Anal. Calcd. for $C_{57}H_{20}Bi_2Cl_{12}I_6N_6O_6$: C, 29.02: H, 0.63: N, 3.76. Found: C, 29.28: H, 1.08: N, 3.70. This was recrystallized by dissolving in CH_2Cl_2 and filtering before layering with warm hexanes (343K). Light brown crystals were formed and filtered (0.802, 71%).

Bis(μ_2-7-bromo-8-hydroxyquinolinato)tetra(7-bromo-8-hydroxyquinolinato)dibismuthine 2-tetrahydrofuran (**5**). Compound **5** was prepared in a similar manner as compound **1** from bismuth (III) chloride (0.315 g, 1 mmol) and 7-

bromo-8-hydroxyquinoline (0.627 g, 3 mmol) in ethanol (60 mL). Triethylamine and deionized water (10 mL) were added to neutralize the HCl produced, and precipitate crude compound. The crude product was purified by layering warm hexanes (343K) over a THF solution. The purified product yielded dark orange crystals (0.430 g, 49%). Elemental analysis of the crude product after drying in vacuo was Anal. Calcd. for $C_{31}H_{23}BiBr_3N_3O_4$: C, 36.93: H, 1.72: N, 4.79. Found: C, 35.44: H, 1.72: N, 4.83.

Tris(2-(diethoxymethyl)-8-quinolinato)bismuth (**6**). Compound **6** was prepared in a similar manner as compound **1** from bismuth (III) chloride (0.315 g, 1 mmol) and-8-hydroxy, 2-quinoline-carboxyaldehyde (0.520 g, 3 mmol) in ethanol (60 mL). Triethylamine and deionized water (10 mL) were added to neutralize the HCl produced, and precipitate **6**. The crude product was purified by dissolving in THF and layering with warm hexanes (343K). This yielded bright, orange crystals (0.519 g, 55%). Anal. Calcd. for $C_{42}H_{48}BiN_3O_9$: C, 53.20: H, 5.11: N, 4.43. Found: C, 52.44: H, 5.31: N, 4.44.

Tris(8-hydroxy-2-quinolinato-carboxylic acid)bismuth (**7**). Compound **7** was prepared in a similar manner as compound **1** with bismuth (III) chloride (0.315 g, 1 mmol) and 8-hydroxy-2-quinoline-carboxylic acid (1.19 g, 3 mmol) in ethanol (60mL). Triethylamine and deionized water (10mL) were added to neutralize the HCl produced, and precipitate crude compound. The crude product was purified in hot THF (323K) and yielded a yellow-orange powder (0.339 g, 44%). Anal. Calcd. for $C_{30}H_{18}BiN_3O_9$: C, 46.59: H, 2.35: N, 5.43. Found: C, 44.87: H, 2.35: N, 6.04.

Tris(8-hydroxy-5-nitroquinolinato)bismuth (**8**). Compound **8** was prepared in a similar manner as compound **1** from bismuth (III) chloride (0.315 g, 1 mmol) and 8-hydroxy-5-nitroquinolinol (1.19 g, 3 mmol) in ethanol (60 mL). Triethylamine and deionized water (10 mL) were added to neutralize the HCl produced, and precipitate **8**. The filter cake was dried under vacuum and yielded a bright yellow powder (0.781 g, 67%). Anal. Calcd. for $C_{27}H_{15}BiN_6O_9$: C, 41.77: H, 1.95: N, 10.82. Found: C, 41.27: H, 1.81: N, 10.69.

Triethylammonium tris(7-iodo-8-hydroxyquinolinato-5-sulfonate)bismuthate (**9**). Bismuth (III) chloride (0.315 g, 1 mmol) was dissolved in 60 mL of degassed THF at room temperature and stirred under an argon atmosphere. 7-iodo-8-hydroxyquinoline-5-sulfonic acid (1.053 g, 3 mmol) was added quickly to the stirring mixture under argon. The yellow solution was refluxed at 323 K for 3 h under argon and then cooled to room temperature. The sulfonic acid groups were neutralized with the addition of triethylamine and then recrystallized by slow evaporation. This yielded bright, yellow-orange crystals (0.887 g, 70%). Anal. Calcd. for $C_{47}H_{66}BiI_3N_6O_{13}S_3$: C, 35.09: H, 4.13: N 5.22. Found: C, 32.80: H, 4.06: N, 5.10.

7.2 *Single X-ray Diffraction Analysis*

All crystals were mounted on Cryoloops with Paratone-N oil. Data for each sample were collected at 100 K with Mo Kα radiation and corrected for absorption with the Siemens Area-detector absorption correction (SADABS). Data for samples compound **4** and **5** were collected with a Bruker Complementary Metal Oxide Sensor (CMOS) detector while data for compound **9** was collected with a Bruker APEX II detector. For all samples, structures were solved by direct methods (SHELXTL) and all non-hydrogen atoms were refined by full matrix least squares on F^2 and all hydrogen atoms were placed in calculated positions with appropriate riding parameters. Solvent disorder was found for compounds **4** and **9**. For compound **4**, one chlorine atom on two of the CH_2Cl_2 solvent molecules were disordered and were refined using a two part (0.38/0.62 and 0.17/0.83) model. For compound **9**, unrefined and diffused solvent THF molecules were treated using the PLATON program SQUEEZE; void volume of 5478 $Å^3$ with 635 electron count. This was treated as being 18 molecules of THF (720e) and the chemical formula was changed to accommodate the change in molecular mass, density and F000 value.

7.3 *Computational Methods*

The density functional theory (DFT) calculations were performed with the Amsterdam Density Functional (ADF) program suite, version 2012.01 using the triple ζ Slater-type orbital basis set. Zero-Order regular approximation (ZORA) was included for relativistic effects in conjunction with the local density approximation of Vosko et al.[37] Generalized gradient approximations for electron exchange and correlation were used as described by Becke and Perdew.[38] Molecular orbitals and final geometries were visualized with ADF-GUI.

Appendix

A. *Solid State Emission Spectra*

Compounds **1-9** were dried under vacuum for 24-48 h before recording the solid-state emission spectra. After thoroughly drying the compounds, they were crushed and spread onto white filter paper as a fine layer. The spectra are for compounds **3, 4, 5,** and **7** are shown in Figure **17**. Compounds **3** and **5** display a green emission around 530 nm in the solid-state. The emission of compound **4** is blue-shifted by 100 nm from compounds **3** and **5**. Compound **4** also has a broad emission peak. Compound **7** has a narrow peak in the green emission at 480 nm. The emission spectra for compounds **5** and **7** also show a small emission peak at around 630-650 nm.

The emission spectra for compounds **6** and **8** (Figure **18**) have dual emission in the solid state. Compounds **1** and **9** have three emission peaks in the solid state. All four compounds have higher energy emission band between 470-550 nm that is similarly seen in the solution emission spectra. Compounds **1, 8** and **9** have a long wavelength peak between 600-700 nm that, like the previous compounds, could be indicative of phosphorescence. Compounds **1, 6,** and **9,** are all monomers in the solid-state and have similar solid-state peaks in the blue-green region of the spectra. The lower intensity peak of tris(5-chloro-8-hydroxyquinolinato)bismuth (**1**) at 490 nm indicates that the Bi-N covalent bond (that gives rise to the blue-shifted emission peaks) could be different in character from those in compounds **6** and **9**.

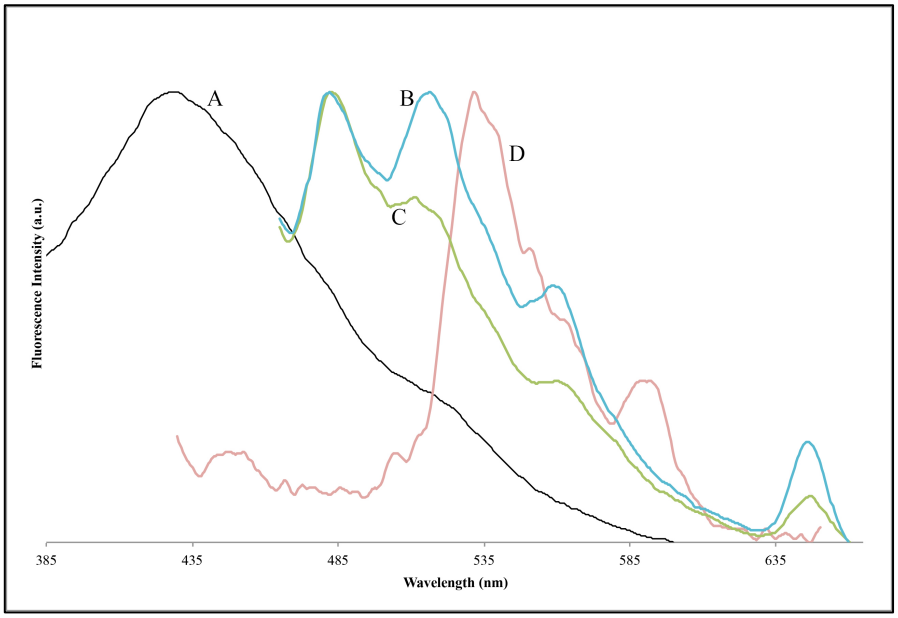

Figure 17. Emission spectra of A) bis(μ_2-5-chloro-7-iodo-8-hydroxyquinolinato)tetra(5-chloro-7-iodo-8-hydroxyquinolinato)dibismuthine (Compound **4**) with an excitation wavelength of 495 nm; B) bis(μ_2-7-bromo-8-hydroxyquinolinato)tetra(7-bromo-8-hydroxyquinolinato)dibismuthine 2-tetrahydrofuran (Compound **5**) with an excitation wavelength of 385 nm; C) tris(8-hydroxy-2-quinolinato-carboxylic acid)bismuth (Compound **7**) with an an excitation wavelength of 389 nm; and D) tris(5,7-diiodo-8-hydroxyquinolinato)bismuth (Compound **3**) with an excitation wavelength of 490 nm. All Emission spectra were taken for powdered compounds dispersed on filter paper at 298K.

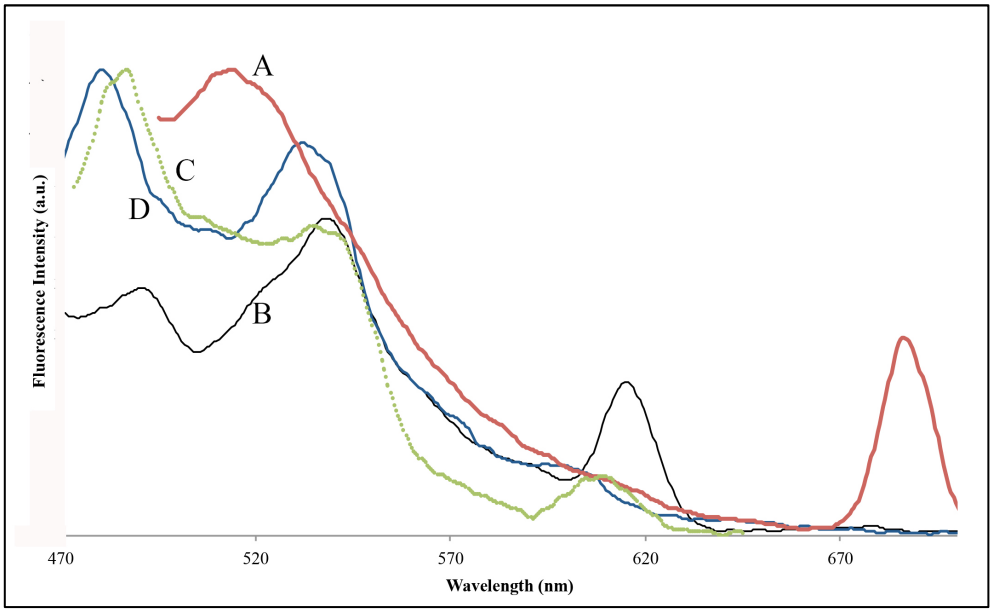

Figure 18. Emission spectra of A) tris(8-hydroxy-5-nitroquinolinato)bismuth (Compound **8**) with an excitation wavelength of 447 nm; B) tris(5-chloro-8-hydroxyquinolinato)bismuth **(**Compound **1**) with an excitation wavelength of 452 nm; C) triethylammonium tris(7-iodo-8-hydroxyquinolinato-5-sulfonate)bismuthate (Compound **9**) with an excitation wavelength of 405 nm; and D) tris(2-(diethoxymethyl)-8-quinolinato)bismuth (Compound **6)**, with an excitation wavelength of 400 nm. All emission spectra were taken of the compounds on filter paper at 298K.

References

(1) Adachi, C.; Baldo, M. A.; Forrest, S. R.; Lamansky, S.; Thompson, M. E.; Kwong, R. C. *Applied Physics Letters* **2001**, *78*, 1622.

(2) Adachi, C.; Baldo, M. A.; Forrest, S. R.; Thompson, M. E. *Applied Physics Letters* **2000**, *77*, 904.

(3) Adachi, C.; Baldo, M. A.; Thompson, M. E.; Forrest, S. R. *Journal of Applied Physics* **2001**, *90*, 5048.

(4) Burrows, P. E.; Sapochak, L. S.; McCarty, D. M.; Forrest, S. R.; Thompson, M. E. *Applied Physics Letters* **1994**, *64*, 2718.

(5) Chen, C. H.; Shi, J. *Coordination Chemistry Reviews* **1998**, *171*, 161.

(6) Utz, M.; Chen, C.; Morton, M.; Papadimitrakopoulos, F. *Journal of the American Chemical Society* **2003**, *125*, 1371.

(7) Montes, V. A.; Pohl, R.; Shinar, J.; Anzenbacher, P. *Chemistry – A European Journal* **2006**, *12*, 4523.

(8) Chen, Z.-F.; Song, X.-Y.; Peng, Y.; Hong, X.; Liu, Y.-C.; Liang, H. *Dalton Transactions* **2011**, *40*, 1684.

(9) Lytle, F. E.; Storey, D. R.; Juricich, M. E. *Spectrochimica Acta Part A: Molecular Spectroscopy* **1973**, *29*, 1357.

(10) Gao, H.-Z.; Su, Z.-M.; Qin, C.-S.; Mo, R.-G.; Kan, Y.-H. *International Journal of Quantum Chemistry* **2004**, *97*, 992.

(11) Halls, M. D.; Schlegel, H. B. *Chemistry of Materials* **2001**, *13*, 2632.

(12) Burrows, P. E.; Shen, Z.; Bulovic, V.; McCarty, D. M.; Forrest, S. R.; Cronin, J. A.; Thompson, M. E. *Journal of Applied Physics* **1996**, *79*, 7991.

(13) Jang, H.; Do, L.-M.; Kim, Y.; Zyung, T.; Do, Y. *Synthetic Metals* **2001**, *121*, 1667.

(14) Popovych, O.; Rogers, L. B. *Spectrochimica Acta* **1959**, *15*, 584.

(15) Rupert, B. L.; Cherepy, N. J.; Sturm, B. W.; Sanner, R. D.; Dai, Z.; Payne, S. A. *MRS Proceedings* **2011**, *1341*.

(16) Rupert, B. L.; Cherepy, N. J.; Sturm, B. W.; Sanner, R. D.; Payne, S. A. *EPL (Europhysics Letters)* **2012**, *97*, 22002.

(17) Baldo, M. A., Thompson, M. E., Forrest, S. R. *Nature* **2000**, *403*, 750.

(18) Braunschweig, H.; Cogswell, P.; Schwab, K. *Coordination Chemistry Reviews* **2011**, *255*, 101.

(19) Freedman, L. D.; Doak, G. O. *Chemical Reviews* **1982**, *82*, 15.

(20) Cherepy, N. J.; Payne, S. A.; Sturm, B. W.; Kuntz, J. D.; Seeley, Z. M.; Rupert, B. L.; Sanner, R. D.; Drury, O. B.; Hurst, T. A.; Fisher, S. E.; IEEE, p 1288.

(21) Moser, S. W.; Harder, W. F.; Hurlbut, C. R.; Kusner, M. R. *Radiation Physics and Chemistry* **1993**, *41*, 31.

(22) Ballardini, R.; Varani, G.; Indelli, M. T.; Scandola, F. *Inorganic Chemistry* **1986**, *25*, 3858.

(23) Hoffmann, R.; Beier, B. F.; Muetterties, E. L.; Rossi, A. R. *Inorganic Chemistry* **1977**, *16*, 511.

(24) Anjaneyulu, O.; Maddileti, D.; Kumara Swamy, K. C. *Dalton Transactions* **2012**, *41*, 1004.

(25) Lawton, S. L.; Fuhrmeister, C. J.; Haas, R. G.; Jarman, C. S.; Lohmeyer, F. G. *Inorganic Chemistry* **1974**, *13*, 135.

(26) Curioni, A.; Boero, M.; Andreoni, W. *Chemical Physics Letters* **1998**, *294*, 263.

(27) DeMasi, A.; Piper, L. F. J.; Zhang, Y.; Reid, I.; Wang, S.; Smith, K. E.; Downes, J. E.; Peltekis, N.; McGuinness, C.; Matsuura, A. *The Journal of Chemical Physics* **2008**, *129*, 224705.

(28) Stavila, V.; Fettinger, J. C.; Whitmire, K. H. *Organometallics* **2007**, *26*, 3321.

(29) Cuvette path length values were standardized at 408 nm with identical concentration samples.

(30) Mann, K. R.; Lewis, N. S.; Williams, R. M.; Gray, H. B.; Gordon, J. G. *Inorganic Chemistry* **1978**, *17*, 828.

(31) Curioni, A.; Andreoni, W. *Journal of the American Chemical Society* **1999**, *121*, 8216.

(32) Humbs, W.; van Veldhoven, E.; Zhang, H.; Glasbeek, M. *Chemical Physics Letters* **1999**, *304*, 10.

(33) Misra, A., Kumar, P., Kumar, L., Dhawan, S.K., Kamalasanan, M. N., Chandra, S. *Indian Journal of Engineering and Material Sciences* **2006**, *12*, 357.

(34) Hopkins, T. A.; Meerholz, K.; Shaheen, S.; Anderson, M. L.; Schmidt, A.; Kippelen, B.; Padias, A. B.; Hall, H. K.; Peyghambarian, N.; Armstrong, N. R. *Chemistry of Materials* **1996**, *8*, 344.

(35) Niedermair, F.; Kwon, O.; Zojer, K.; Kappaun, S.; Trimmel, G.; Mereiter, K.; Slugovc, C. *Dalton Transactions* **2008**, 4006.

(36) Tsaryuk, V.; Zhuravlev, K.; Zolin, V.; Gawryszewska, P.; Legendziewicz, J.; Kudryashova, V.; Pekareva, I. *Journal of Photochemistry and Photobiology A: Chemistry* **2006**, *177*, 314.

(37) Vosko, S. H.; Wilk, L.; Nusair, M. *Canadian Journal of Physics* **1980**, *58*, 1200.

(38) Becke, A. D. *Physical Review A* **1988**, *38*, 3098.